Annals of Nuclear Energy 120 (2018) 348–366

Contents lists available at ScienceDirect

Annals of Nuclear Energy

journal homepage: www.elsevier.com/locate/anucene

Validating the performance of correlated fission multiplicity implementation in radiation transport codes with subcritical neutron multiplication benchmark experiments

Jennifer Arthur [a,b,*], Rian Bahran [a], Jesson Hutchinson [a], Avneet Sood [a], Michael Rising [a], Sara A. Pozzi [b]

[a] Los Alamos National Laboratory, Los Alamos, NM 87545, United States
[b] University of Michigan Department of Nuclear Engineering and Radiological Sciences, Ann Arbor, MI 48109, United States

ARTICLE INFO

Article history:
Received 20 March 2018
Received in revised form 25 May 2018
Accepted 28 May 2018
Available online 14 June 2018

Keywords:
Fission multiplicity
Radiation transport
Subcritical benchmark
Neutron multiplication

ABSTRACT

Historically, radiation transport codes have uncorrelated fission emissions. In reality, the particles emitted by both spontaneous and induced fissions are correlated in time, energy, angle, and multiplicity. This work validates the performance of various current Monte Carlo codes that take into account the underlying correlated physics of fission neutrons, specifically neutron multiplicity distributions. The performance of 4 Monte Carlo codes - MCNP®6.2, MCNP®6.2/FREYA, MCNP®6.2/CGMF, and PoliMi - was assessed using neutron multiplicity benchmark experiments. In addition, MCNP®6.2 simulations were run using JEFF-3.2 and JENDL-4.0, rather than ENDF/B-VII.1, data for ^{239}Pu and ^{240}Pu. The sensitive benchmark parameters that in this work represent the performance of each correlated fission multiplicity Monte Carlo code include the singles rate, the doubles rate, leakage multiplication, and Feynman histograms. Although it is difficult to determine which radiation transport code shows the best overall performance in simulating subcritical neutron multiplication inference benchmark measurements, it is clear that correlations exist between the underlying nuclear data utilized by (or generated by) the various codes, and the correlated neutron observables of interest. This could prove useful in nuclear data validation and evaluation applications, in which a particular moment of the neutron multiplicity distribution is of more interest than the other moments. It is also quite clear that, because transport is handled by MCNP®6.2 in 3 of the 4 codes, with the 4th code (PoliMi) being based on an older version of MCNP®, the differences in correlated neutron observables of interest are most likely due to the treatment of fission event generation in each of the different codes, as opposed to the radiation transport.

1. Introduction

Experts in the fields of nuclear nonproliferation, safeguards, and criticality safety have been continually performing subcritical special nuclear material (SNM) measurements since the 1940s. The results of these experiments have provided data used for simulations of SNM systems. Improvements in nuclear detection instrumentation and SNM availability in the 1950s and 1960s lead to increased research activity in both the theory and practice of multiplication and reactivity measurements. Neutron multiplication is an extremely important parameter in SNM systems, as it can give information about the type, enrichment, and risk level of the SNM being investigated for nuclear security reasons. In addition, for criticality safety purposes, it is extremely important to be able to accurately predict the multiplication of systems for various processes and experiments. Neutron multiplication inference measurements take advantage of the fact that neutrons emitted during fission are correlated in time and can be used to gain knowledge about the system being measured. Multiplying system parameters of interest include neutron leakage multiplication M_L, total neutron multiplication M_T, the neutron multiplication factor k_{eff}, and the prompt neutron multiplication factor k_p. M_L represents the average number of prompt neutrons escaping a system for every neutron injected into the system, while M_T represents the number of prompt neutrons created on average by a single neutron in the multiplying system. k_{eff} is a measure of the ratio of the total number of neutrons in the current fission generation to the total number of neutrons in the previous generation. k_p is a measure of the ratio of the number of prompt neutrons in the current fission generation to the number of prompt neutrons in the previous

* Corresponding author at: Los Alamos National Laboratory, Los Alamos, NM 87545, United States.
E-mail address: jennifera@lanl.gov (J. Arthur).

https://doi.org/10.1016/j.anucene.2018.05.051
0306-4549/

generation. Some subcritical inferred neutron multiplication parameters of interest are sensitive to the distribution of the number of neutrons emitted per fission. Comparisons between subcritical neutron multiplication inference measurements and simulations have been used to validate multiplication inference techniques and radiation particle transport codes, and to identify and correct deficiencies in underlying nuclear data quantities such as $\bar{\nu}$ (average number of prompt neutrons emitted per fission) (Arthur et al., 2016; Bahran et al., 2014; Sood et al., 2014; Bolding and Solomon, 2013; Miller et al., 2010; Mattingly et al., 2009; Bahran et al., 2014; Boldeman and Hines, 1985). Most notably, recent (1990s and 2000s) methods of obtaining list mode data (time stamps of neutron events registered in a detector) from both measurements and simulations have also been developed and allow for a more detailed comparison between the two (Hutchinson et al., 2016).

More recently, there has been significant progress on the design and execution of benchmark quality subcritical neutron multiplication measurements for radiation transport code and nuclear data validation. The majority of these experiments have involved a 4.5 kg alpha-phase plutonium sphere (BeRP ball) surrounded by copper (Bahran and Hutchinson, 2016), tungsten (Richard et al., 2016), and nickel (Richard et al., 2016). The International Criticality Safety Benchmark Evaluation Project (ICSBEP) Handbook (Briggs, 2014) includes accepted evaluations of both the nickel and tungsten measurements. The ICSBEP handbook contains thousands of critical and subcritical measurement benchmark evaluations. The purpose of the handbook is to provide trusted benchmarks for validation and improvement of nuclear databases and radiation transport codes. The nickel benchmark was the first ICSBEP-accepted evaluation of measurements analyzed with the Hage-Cifarelli formalism based on the Feynman Variance-to-Mean method (Cifarelli and Hage, 1986), and was the culmination of many years of collaborative subcritical experiment research (Arthur et al., 2016; Bahran et al., 2014; Sood et al., 2014; Bolding and Solomon, 2013; Miller et al., 2010; Mattingly et al., 2009; Hutchinson et al., 2016; Richard et al., 2016; Richard et al., 2016; Hutchinson et al., 2013; Hutchinson et al., 2014; Hutchinson et al., 2013; Hutchinson et al., 2015).

This work investigates the performance of various current Monte Carlo codes that take into account at least some of the correlated physics of fission neutrons (i.e. correlations in time, energy, angle, or some combination of the three). Historically, radiation transport codes have uncorrelated fission emissions. In reality, both spontaneous and induced fissions release particles that are correlated in time, energy, angle, and multiplicity. The fission process can be either spontaneous or initiated by an interacting neutron. In the case of spontaneous fission, the nucleus is inherently unstable and randomly decays by fission. In the case of neutron-induced fission, an unstable compound nucleus forms after an incident neutron collides with the original nucleus. In either case, the nucleus scissions into two fission fragments, which receive some of the energy liberated from the rearrangement of mass as kinetic energy. The fission fragments release the remaining energy in the form of prompt neutron emission, prompt gamma ray emission, and delayed β or electron conversion decay. Because the particles are emitted from moving fission fragments, the multiplicities, energies, and angles of emission of prompt neutrons and gamma rays are dependent upon both each other and the initial masses and kinetic energies of the fission fragments (Wagemans, 1991). For this work, only prompt fission neutrons are of interest and the authors do not consider the physics of gamma production in fission. Because of their large impact on correlated neutron results, this work also compares underlying fission neutron multiplicity distributions utilized by the different codes.

2. Correlated fission multplicity

2.1. Nuclear data

For the purposes of this paper we will be focusing on the nuclear reaction database utilized by the general purpose Monte Carlo code MCNP®6.2[1], namely the Evaluated Nuclear Data File (ENDF) (Chadwick et al., 2011), although results will also be obtained using the Joint Evaluated Fission and Fusion File (JEFF) (Santamarina et al., 2009) and the Japanese Evaluated Nuclear Data Library (JENDL) (Shibata et al., 2011). ENDF contains information related to the types and probabilities of the different possible reactions between radiation particles and various isotopes. Evaluators use data from high-quality differential measurements to evaluate nuclear data libraries such as ENDF, and comparisons of simulated and measured data from benchmark-quality integral measurements to validate the libraries. Fig. 1 summarizes the process. Included in the information provided by ENDF are data summarizing both the probability of fission occurring and the average number of neutrons released per fission of each fissionable isotope, represented as $\bar{\nu}$, as functions of incident neutron energy. The multiplicity distribution $P(\nu)$ represents the probability for ν neutrons to be emitted per fission. Complete multiplicity distributions, $P(\nu)$, are not included in ENDF/B-VII.1; correlations in angle and energy are also not included.

Overall, the ENDF evaluation process focuses on complying as closely as possible with differential experimental data contained in the CSISRS (or EXFOR) database (NRDC-Network, 2017), while simultaneously showing general agreement with critical benchmark measured data. Evaluators did not make any changes to $\bar{\nu}$ between the previous evaluation (ENDF/B-VII.0) and the current evaluation (ENDF/B-VII.1) (Chadwick, 2006). Therefore, the evaluation process of the ENDF/B-VII.0 version will be described with regard to $\bar{\nu}$. For the ENDF/B-VII.0 evaluation, the experimental database from the ENDF/B-VI evaluation was used, with corrections to the normalization of the $\bar{\nu}$ nuclear data. This resulted in evaluations that match well with the corrected experimental database for ^{235}U, ^{238}U and ^{239}Pu. Appreciable deviation from experimental data occurs in the energy range below 1.5 MeV for ^{239}Pu, and this is partially due to the desire to match JEZEBEL (a LANL fast critical benchmark experiment) results in particular (Chadwick, 2006).

One of the main parameters of interest that is used to validate ENDF is the effective multiplication factor k_{eff}, which is sensitive to $\bar{\nu}$ but not to the other moments of the $P(\nu)$ distribution. The effective multiplication factor is in general insensitive to changes in the correlated physics of fission and depends only on averages. This can be illustrated by examining the neutron transport equation, which consists of terms representing the loss of neutrons due to leakage out of the system, the loss of neutrons due to all interactions, the addition of neutrons due to in-scattering from another energy group, and the production of neutrons due to fission. Only the average quantity $\bar{\nu}(E)$ is required to calculate neutron transport and the effective multiplication factor of a system. However, by looking at the Hage-Cifarelli equation for the leakage multiplication of a system, in Eqs. (11) and (12), which are presented and explained later in this work, it is clear that other moments of the multiplicity distribution (ν_{s2}, ν_{I2}) are also important.

The average number of neutrons released per fission is a specific measured observable of some of the differential measurements of fission product yields, masses, and fission neutron energy spectra contained in EXFOR. Because of the contribution of neutrons from

[1] MCNP® and Monte Carlo N-Particle® are registered trademarks owned by Los Alamos National Security, LLC, manager and operator of Los Alamos National Laboratory.

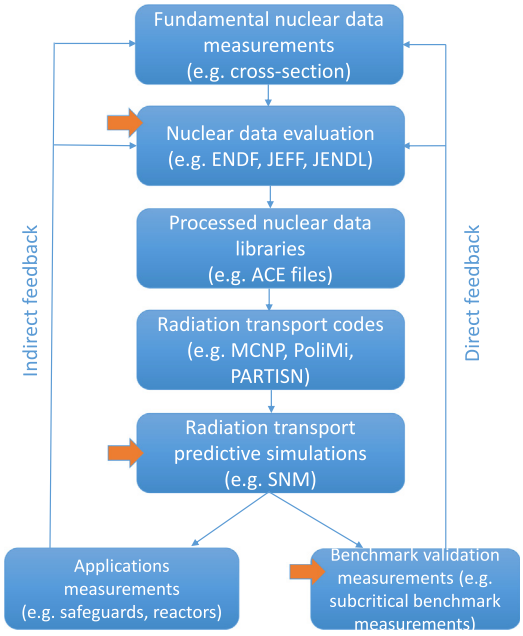

Fig. 1. The nuclear data evaluation and validation process. Arrows indicate the steps in the process that this work focuses on.

interactions other than fission, it is difficult to measure characteristics of the fission neutrons only, such as the spectra or the number released per fission, especially at high incident neutron energies. In addition, some actinides are not readily available in a very pure isotopic concentration, and impurities affect the observed yields. Methods such as time-of-flight, multiplicative transmission through a fissionable target, and gamma-ray spectroscopic techniques have been used to measure fission yields, but overall few measurements of this type have been conducted. As a result of the lack of reliable differential fission yield measurements, semi-empirical calculations and systematic fission models have been used by nuclear data evaluators (Barnard et al., 1965; Flerov and Talyzin, 1960; Iyer et al., 2000; Naika et al., 2013; Howerton, 1977; Madland and Nix, 1982; Holden and Zucker, 1988; Rising, 2013). Thus, integral measurements that are sensitive to the nuclear data corresponding to fission yields, such as $\bar{\nu}$ and fission neutron energy spectra, are very important for fission yield nuclear data validation and evaluation.

The goal of this work is to apply subcritical ICSBEP benchmarks to comparisons of measured correlated neutron observables, and simulated observables generated by various Monte Carlo (MC) radiation transport codes that take into account various parts of the correlated physics of fission neutrons. Such comparisons will offer a type of validation that has never before been considered in nuclear data evaluation. In addition, this work investigates the effects of the different multiplicity distributions used by various MC codes on correlated neutron observables of interest.

2.2. Implementation in transport codes

The Monte Carlo radiation transport codes that this work currently compares include MCNP (Goorely, 2012), MCNP/FREYA (Rising et al., 2014; Hagmann, 2013), MCNP/CGMF (Talou, 2013), and PoliMi (Pozzi, 2012; Pozzi et al., 2003). The first few of these codes are specific releases of or options contained in the Monte Carlo N-Particle (MCNP) code, the precursors of which were originally developed during the Manhattan Project era to simulate neutron diffusion and multiplication in fissioning systems (Goorely, 2012). Diffusion and multiplication depend on average quantities only, and do not require modeling of the correlated physics of fission. Therefore, the correlated physics of fission was irrelevant for the Monte Carlo transport code developers at that time, and average parameters such as $\bar{\nu}$ were sufficient to simulate the fission process. However, with the increasing interest in nuclear security, safeguards, and nonproliferation, experimenters are desiring extremely accurate predictive modeling of SNM measurements. SNM has correlated fission emissions, and therefore average event treatment is not always sufficient for these applications. This work investigates various codes that are able to handle correlated fission quantities of interest, such as spontaneous and induced fission multiplicity distributions.

By default, MCNP uses a bounded integer treatment and the $\bar{\nu}$ data from ENDF to sample the number of neutrons emitted from each simulated fission event. In the bounded integer treatment, the two integers bounding $\bar{\nu}$ are the only values of ν that are sampled, instead of a complete multiplicity distribution. The FMULT card, an optional input in MCNP that allows for user definition of spontaneous and induced fission parameters, can be utilized to call either built-in or user-specified multiplicities to replace the bounded integer treatment (MCNP6, 2013). The user can also use the FMULT card to call either the Fission Reaction Event Yield Algorithm (FREYA) or the Cascading Gamma-Ray Multiplicity with Fission (CGMF) fission event generating codes to handle fission. The FREYA fission event generator determines the number, energy, and direction of particles emitted for each fission event and gives the results to MCNP for transport. The fission event generator uses fission fragment mass and kinetic energy distributions, unbounded statistical evaporation models, and conservation of energy and momentum to generate the number, energy, and direction of neutrons released by each fission event using the Monte Carlo Weisskopf approach. The Weisskopf approach repeatedly samples emitted neutron parameters from the Weisskopf distribution, until the remaining fission fragment excitation energy is below a specified threshold. This fission fragment then releases the remaining excitation energy in the form of fission gamma rays. Eqs. (1)–(3) describe the sampling process of emitted neutrons. Eq. (1) is used to calculate the maximum temperature of the evaporated neutron from the Q-value for neutron emission (Q_n) and the level-density parameter of the fission fragment nucleus (a_d). The neutron kinetic energy in the center of mass frame (ϵ_n) is then sampled from Eq. (2). Finally, the new excitation energy of the fission fragment is recalculated using Eq. (3), and the process repeats until E_d^* falls below the specified excitation energy threshold (Hagmann, 2013; Rising et al., 2014; Verbeke et al., 2015; Verbeke et al., 2016).

$$a_d T_{max}^2 = Q_n \tag{1}$$

$$f_n(\epsilon_n) \sim \epsilon_n exp\left(\frac{-\epsilon_n}{T_{max}}\right) \tag{2}$$

$$E_d^* = Q_n - \epsilon_n \tag{3}$$

CGMF generates prompt fission neutrons using the statistical Hauser-Feshbach formalism (Hauser and Feshbach, 1952; Talou, 2013), which is the primary difference between FREYA and CGMF, and gives results to MCNP for transport. The Hauser-Feshbach approach accounts for the competition between neutrons and gamma rays emitted during the fission process. It is therefore technically a more complete fission model, but significantly increases computational time. Eq. (4) is used to sample the emitted neutron kinetic energies, and makes use of transmission coefficients (T_n) calculated using optical models. In this equation $\rho(Z, A-1, E-\epsilon_n-S_n)$ is the level density of the fission fragment nucleus after the neutron is emitted (Z is the atomic number,

and $A-1$ is the new atomic mass), using the remaining available excitation energy (the original excitation energy E, minus the emitted neutron kinetic energy ϵ_n and the neutron separation energy S_n) (Talou, 2013; Rising et al., 2014).

$$P(\epsilon_n)dE \propto T_n(\epsilon_n)\rho(Z, A-1, E-\epsilon_n-S_n) \quad (4)$$

PoliMi utilizes a few different built-in multiplicity sets, and also models both the angular anisotropy and multiplicity-dependent energy spectra of neutrons emitted in spontaneous fission. The user is able to choose which spontaneous and induced fission built-in multiplicity distributions to use, and whether or not to turn on the modeling of angular anisotropy in spontaneous fission sources (Padovani et al., 2012; Santi and Miller, 2008; Terrell, 1957).

3. Benchmark experiments

3.1. Inferred multiplication benchmarks

Historically, criticality safety has always been a concern for those working with systems containing nuclear material. In the early years of the nuclear industry, physical experiments were used to answer questions pertaining to criticality safety. Then, analytic calculations were performed using computers. Finally, Monte Carlo radiation transport simulation techniques were developed that allowed for accurate modeling of complex multi-dimensional systems. Because of this, validation of radiation transport codes and associated basic nuclear data through comparisons with integral experimental data became an issue of importance to the criticality safety field. Experimenters executed many measurements, but these measurements lacked quality assurance and sufficient documentation. ICSBEP was created by the United States Department of Energy in 1992 to satisfy this need for systematic evaluation and documentation of integral experimental data, and the Organisation for Economic Cooperation and Development (OECD) - Nuclear Energy Agency (NEA) took on the project as one of its official duties in 1995 (Briggs, 2014; Briggs, 2003). The ICSBEP handbook contains thousands of benchmark quality critical and subcritical measurement evaluations from Argentina, Brazil, Canada, China, the Czech Republic, France, Germany, Hungary, India, Japan, Kazakhstan, Poland, Russia, Serbia, Slovenia, Spain, Sweden, the United Kingdom, and the United States. The purpose of the handbook is to provide peer-reviewed benchmark quality data for validation and improvement of nuclear databases and radiation transport codes, specifically codes that calculate the effective neutron multiplication factor (Briggs, 2014; Briggs, 2003). Several of the included measurements involve inferred multiplication measurements, wherein list-mode data is used to calculate leakage multiplication from the sample of interest. The result can then be compared to both criticality and fixed source Monte Carlo calculations for validation purposes. Raw list-mode data and other parameters of interest can also be compared.

3.2. Reflected plutonium benchmark series

In recent years Los Alamos National Laboratory (LANL) has performed several reflected plutonium benchmark experiments (Hutchinson and Loaiza, 2007; Richard et al., 2016; Richard et al., 2016; Hutchinson et al., 2017). In this study, performance of the different codes is compared using various plutonium metal benchmark cases. The growing database of subcritical neutron multiplication inference benchmark experiments includes recent benchmark experiments with a 4.5 kg α-phase plutonium sphere (BeRP ball) surrounded by copper (Hutchinson et al., 2017), tungsten (Richard et al., 2016), and nickel (Richard et al., 2016). Evaluations of the measurements were the first ICSBEP-accepted evaluations of measurements using the Feynman Variance-to-Mean method. This was the culmination of many years of subcritical experiment research, including measurements in 2009 by Sandia National Laboratory (Mattingly et al., 2009; Miller, 2012) which showed a marked sensitivity of subcritical leakage multiplication to the full ^{239}Pu induced fission multiplicity distribution, and indicated the possible existence of nuclear data deficiencies (Hutchinson et al., 2016).

The available BeRP benchmark MCNP models have been adjusted to be compatible with the other codes while maintaining the original measurement geometries. The measured benchmark results are also available for comparison. The typical reflected plutonium subcritical benchmark measurement setup involves the BeRP ball surrounded by various thickness of metal reflectors, with multiplicity detectors 50 cm on either side, as shown in Fig. 2. The BeRP-Ni benchmark geometry consists of the BeRP ball surrounded by various thicknesses of nickel reflectors, ranging from 0 in. to 3.0 in., with a LANL ^{3}He multiplicity detector (NPOD) 50 cm away on either side, as shown in Fig. 3. The BeRP-W benchmark consists of the BeRP ball surrounded by various thicknesses of tungsten reflectors, ranging from 0 in. to 3.0 in., with an NPOD 50 cm away on either side, as shown in Fig. 4. The NPOD consists of 15 ^{3}He neutron detectors inside a polyethylene moderator, and is a predecessor to the currently used NoMAD (Moss et al., 2016; Richard et al., 2016; Richard et al., 2016).

4. Data analysis method

4.1. Multiplicity distributions

The ^{239}Pu neutron induced fission and ^{240}Pu spontaneous fission multiplicity distributions $P(\nu)$ used by all of the codes are investigated for comparison purposes. Because this work focuses on BeRP ball experiments, all induced fissions are assumed to be of ^{239}Pu, and all spontaneous fissions of ^{240}Pu. This is because, at the time of both the BeRP-Ni and BeRP-W experiments, the ^{239}Pu and ^{240}Pu atomic fractions in the BeRP ball were 9.260E-01 and 5.838E-02, respectively, with the next largest actinide atomic fraction being 2.527E-03 (^{241}Am). In addition, the percentage of spontaneous fission neutrons coming from ^{240}Pu was calculated to be 98.5% (Richard et al., 2016; Richard et al., 2016). The singles, doubles, and Feynman histogram results are expected to be sensitive to differences in the underlying multiplicity distributions. User-defined MCNP and PoliMi distributions are obtained from Lestone (Lestone, 2005), Santi (Santi and Miller, 2008), and Terrell (Terrell, 1957). Multiplicity distributions are specified as either a cumulative distribution function (CDF) or as a Gaussian mean ($\bar{\nu}$) and width (σ). If the distribution is given as a CDF, the probability distribution function (PDF) and mean and width are solved for. If the distribution is given as a Gaussian mean and width, the PDF is calculated. In the case of induced fission multiplicity distributions for MCNP and PoliMi, the means are obtained as a function of incident neutron energy from the nuclear data library ENDF/B-VII.1 and only the widths come from the above references. MCNP/FREYA and MCNP/CGMF $P(\nu)$, which are produced by the fission event generator of the code rather than being pulled from a pre-existing multiplicity distribution, are extracted from the particle track (PTRAC) file. The PTRAC file gives the individual ν for each fission, from which a frequency distribution is formed. The Gaussian mean and width are calculated from the frequency distribution, which is treated as a PDF.

The spontaneous and neutron induced fission (at 2 MeV incident neutron energy) multiplicity distributions for each code were obtained from Lestone, Santi, and Terrell (Lestone, 2005; Santi and Miller, 2008; Terrell, 1957), as well as the ENDF/B-VII.1 library and

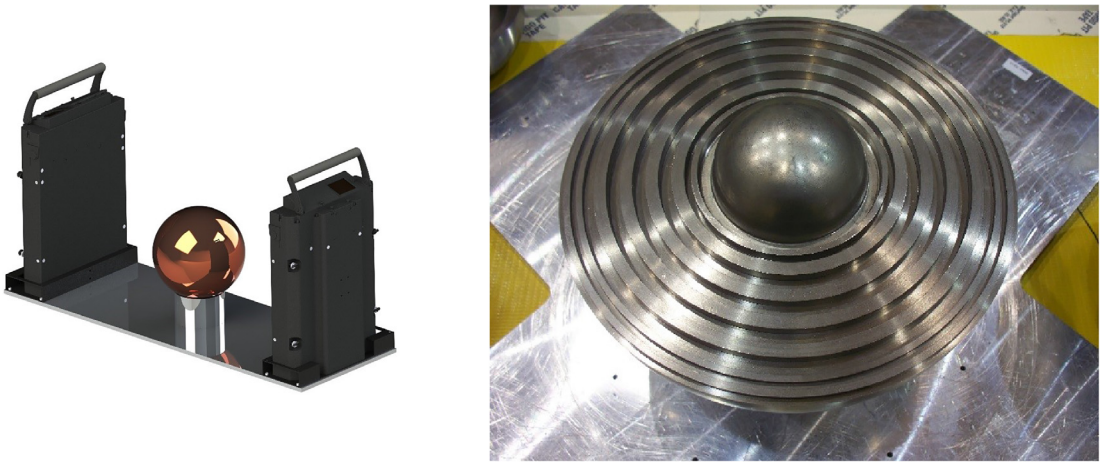

Fig. 2. CAD image of a typical reflected plutonium setup (left), and picture of the BeRP ball within metal reflector shells (right).

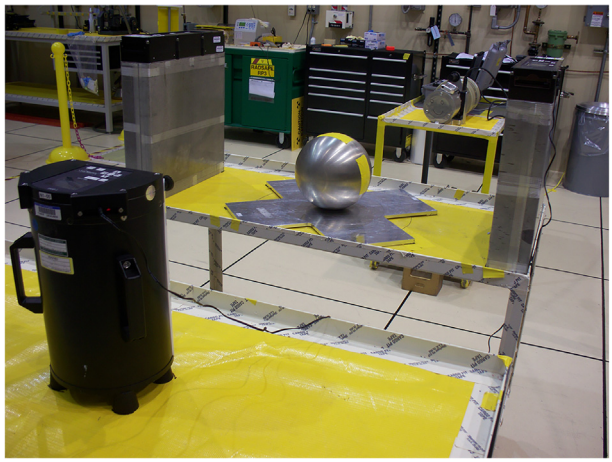

Fig. 3. Picture of the BeRP-Ni benchmark experiment being conducted at the National Criticality Experiments Research Center (NCERC).

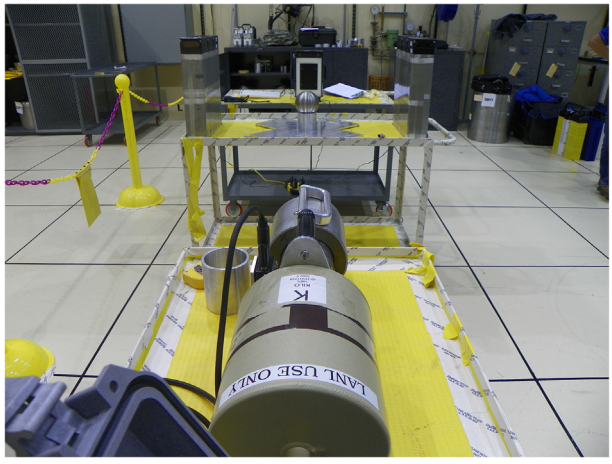

Fig. 4. Picture of the BeRP-W benchmark experiment being conducted at NCERC.

the PTRAC output file. Fig. 5 shows plots of the multiplicity distributions, with tabular versions of the data given in Table 1. 2 MeV was chosen as a representative energy for induced fission due to the fact that the average energy of neutrons causing fission in the bare BeRP system is 1.98 MeV (Richard et al., 2016). To obtain an isolated 2 MeV induced fission multiplicity distribution for MCNP/FREYA and MCNP/CGMF, PTRAC files resulting from simulations of an isotropic 2 MeV neutron source hitting a thin film of pure ^{239}Pu were used.

Table 1 shows that the first moment of the spontaneous fission multiplicity distribution is significantly higher for CGMF compared to all of the other codes, while the first moment of the induced fission multiplicity distribution is significantly lower for FREYA. In addition, the standard deviation (the square root of the second moment) of the spontaneous fission multiplicity distributions are much higher for Lestone and Santi than for the fission event generators (FREYA and CGMF), while the standard deviations of the induced fission multiplicity distribution are more clustered together. Differences in $P(\nu)$ are likely a cause of discrepancies in Feynman histograms and doubles rates. Singles rates are expected to change only with the mean of the multiplicity distribution, $\bar{\nu}$, rather than with both the mean and the width (standard deviation), σ. This is expected because the singles and doubles rates depend on the first and second factorial moments of the binned list-mode data, respectively (see next section).

4.2. List-mode data and Feynman analysis

List-mode data, containing the time and detector tube corresponding to the particle interaction, are obtained from the PTRAC output files of MCNP, and the collision data file of PoliMi. The list-mode data is binned into Feynman histograms according to specified time widths using the data processing tool Momentum (Smith-Nelson, 2015). A Feynman histogram is a representation of the relative frequencies of various multiplets (i.e., 1 event, 2 events, etc.) occurring within the specified time width, as illustrated in Fig. 6.

The magnitude of the nth bin of the Feynman histogram at the specified time width τ is represented by the variable $C_n(\tau)$ in Eq. (5). Standard multiplicity equations, in the form of Eqs. (5)–(12) (Hutchinson et al., 2015), are applied to calculate the singles (R_1) and doubles (R_2) rates, as well as the leakage multiplication (M_L). The values C_1, C_2, and C_3 in Eq. (12) are unrelated to the $C_n(\tau)$ in Eq. (5). It should be noted that the derivation of these equations includes the assumption that the contribution of neutrons from (α, n) reactions is negligible, which is an acceptable assumption for plutonium metal systems such as the metal-reflected BeRP ball. The "singles" rate is defined as the rate of detection of single neutrons from a fission chain.

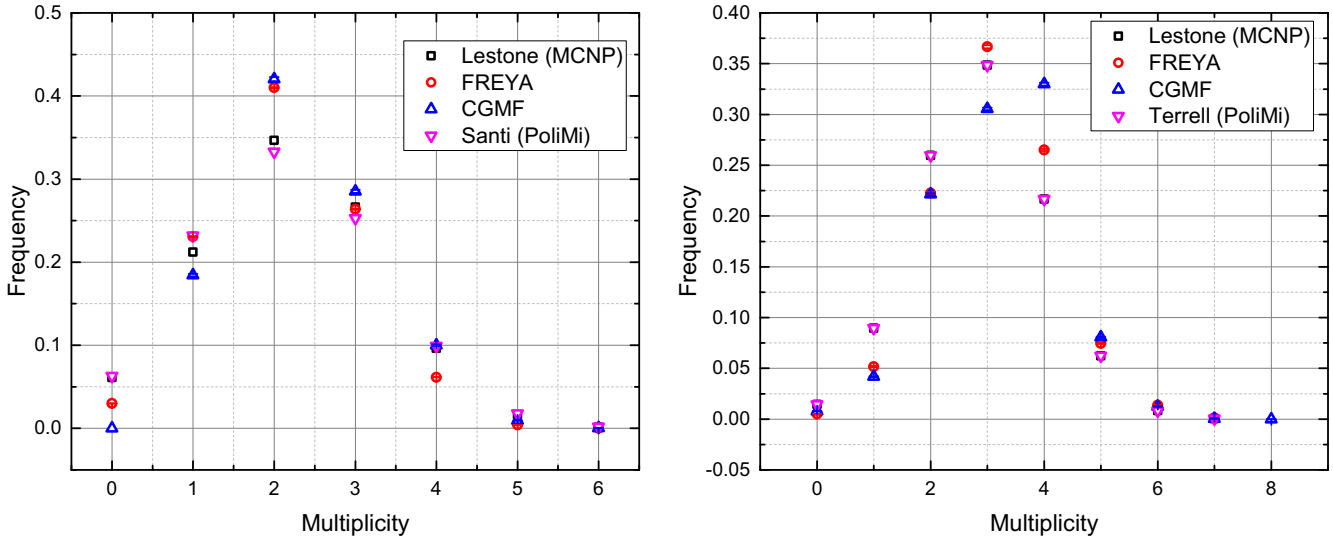

Fig. 5. ^{240}Pu spontaneous fission (left) and^{239}Pu induced fission at 2 MeV incident neutron energy (right) multiplicity distributions utilized by the various codes.

Table 1
^{240}Pu spontaneous fission (SF) and ^{239}Pu induced fission (IF) multiplicity distribution parameters utilized by the various codes.

Code	SF $\bar{\nu}$	SF σ	IF $\bar{\nu}$	IF σ
MCNP	2.151 (Lestone)	1.151 (Lestone)	3.178 (ENDF)	1.140 (Lestone)
MCNP/FREYA	2.109	0.942	3.128	1.057
MCNP/CGMF	2.225	0.949	3.202	1.191
PoliMi	2.093 (Santi)	1.199 (Santi)	3.178 (ENDF)	1.140 (Terrell)

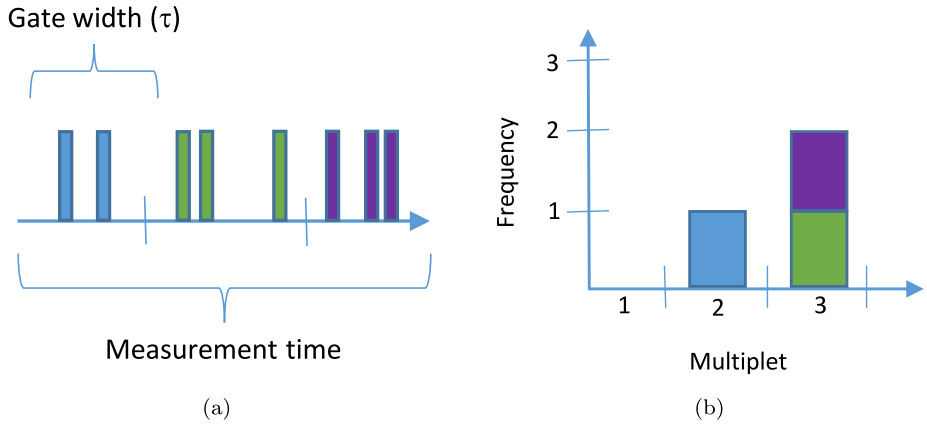

Fig. 6. The binning method (a) used to generate Feynman histograms (b) in this work.

The "doubles" rate is defined as the rate of detection of two neutrons from the same fission chain. Leakage multiplication is the number of neutrons escaping a multiplying system per a single neutron injected into the system. In the following equations the symbols λ, ϵ , ν_{li} and ν_{si} represent the inverse neutron lifetime, detector absolute efficiency, ith factorial moment of the induced fission multiplicity distribution, and ith factorial moment of the spontaneous fission multiplicity distribution, respectively. Y_2 is directly proportional to the Feynman Y value, which is a measure of the deviation of the histogram from a Poisson distribution.The inverse of the neutron lifetime can be obtained by fitting the curve of Y_2 versus time width, because Y_2 is proportional to ω_2 (Cifarelli and Hage, 1986). The inverse of the neutron lifetime is then used as an input to ω_2. Table 2 lists the most commonly used units for many of the variables presented in this section.

Table 2
Most commonly used units for many of the variables used in this work for correlated neutron detection.

Variable	Units
τ	μs
$C_n(\tau)$	# of occurrences
$R_1(\tau)$	s^{-1}
$R_2(\tau)$	s^{-1}
λ	s^{-1}
ϵ	unitless
M_L	unitless

$$p_n(\tau) = \frac{C_n(\tau)}{\sum_{n=0}^{\infty} C_n(\tau)} \tag{5}$$

$$m_r(\tau) = \frac{\sum_{n=0}^{\infty} n(n-1)\dots(n-r+1)p_n(\tau)}{r!} \tag{6}$$

$$R_1(\tau) = \frac{m_1(\tau)}{\tau} \tag{7}$$

$$Y_2(\tau) = \frac{m_2(\tau) - \frac{1}{2}[m_1(\tau)]^2}{\tau} \tag{8}$$

$$\omega_2(\lambda,\tau) = 1 - \frac{1-e^{-\lambda\tau}}{\lambda\tau} \tag{9}$$

$$R_2(\tau) = \frac{Y_2(\tau)}{\omega_2(\lambda,\tau)} \tag{10}$$

$$M_L = \frac{-C_2 + \sqrt{C_2^2 - 4C_1C_3}}{2C_1} \tag{11}$$

$$C_1 = \frac{\nu_{s1}\nu_{I2}}{\nu_{I1}-1},\ C_2 = \nu_{s2} - \frac{\nu_{s1}\nu_{I2}}{\nu_{I1}-1},\ C_3 = -\frac{R_2(\tau)\nu_{s1}}{R_1(\tau)\epsilon} \tag{12}$$

4.3. Uncertainty and correlation analysis

Uncertainties associated with the multiplicity distributions obtained from simulation output files are calculated using Poisson counting statistics (because radioactive decay is a Poissonian process, the predicted standard deviation can be calculated as the square root of the experimental mean (Knoll, 2010)). The uncertainty associated with each possible number of neutrons emitted during fission is equal to the square root of the number of times the given number of neutrons was emitted in the simulation. Feynman histogram uncertainties are also calculated using Poisson counting statistics. The uncertainty associated with each bin in the histogram is equal to the square root of the number of multiplets in the given bin. Reference (Hutchinson et al., 2015) contains equations for the uncertainties in R_1, R_2, and M_L. All uncertainties for other derived quantities (such as (C-E)/E) are calculated using standard uncertainty propagation, according to Eq. (13).

$$\sigma_z^2 = \left(\frac{\delta z}{\delta x}\right)^2 \sigma_x^2 + \left(\frac{\delta z}{\delta y}\right)^2 \sigma_y^2 + \dots \tag{13}$$

In order to investigate the existence of correlation between different observables and nuclear data items of interest, the Pearson correlation coefficient was used. Eq. (14) is used to calculate the sample Pearson correlation coefficient. If $r = -1, r = 0$, or $r = 1$, then x and y are considered to be completely anti-correlated, completely uncorrelated, or completely correlated, respectively. As applied to this work, each sample consists of a single observable and single nuclear data item for a single configuration of a single benchmark experiment, across all of the different radiation transport codes being compared.

$$r = \frac{\sum_{i=1}^{n}(x_i - \bar{x})(y_i - \bar{y})}{\sqrt{\sum_{i=1}^{n}(x_i - \bar{x})^2}\sqrt{\sum_{i=1}^{n}(y_i - \bar{y})^2}} \tag{14}$$

As applied to this work, in Eq. (14), n is the number of codes being compared, x_i is the value of a single observable of interest for the ith code, y_i is the value of a single nuclear data item of interest for the ith code, $\bar{x}$ is the mean of all values of x, and $\bar{y}$ is the mean of all values of y. Because this work includes 3 observables of interest (R_1, R_2, and M_L), 4 nuclear data items of interest (SF and IF $\bar{\nu}$ and σ), and 8 different configurations of the BeRP-W benchmark, 96 values of r exist.

5. Results

5.1. Multiplicity distributions

Fig. 7 shows induced fission multiplicity distributions for a few representative configurations of the BeRP-W benchmark for MCNP, MCNP/FREYA, MCNP/CGMF, and PoliMi. The induced fission multiplicity distributions include all incident neutron energies and are obtained from the PTRAC output files for MCNP based codes, and the collision output file for PoliMi. The multiplicity distribution mean ($\bar{\nu}$) and width (σ) values in Table 3 were obtained using the statistical definitions of mean and standard deviation. Appendix A plots the multiplicity distribution means and widths across all BeRP-W configurations.

As expected, the widths of the MCNP and PoliMi distributions do not change for different energies (reflector thicknesses). Overall, the means decrease slightly with decreasing energy, as do the widths for MCNP/FREYA and MCNP/CGMF. The multiplicity distributions do not vary much for the different reflector thicknesses because the neutron energy spectrum remains quite fast for all configurations. Between codes $P(\nu)$ is similar, with most discrepancies being located to the center of the distribution. Regarding the discrepancies between $P(\nu)$ for the fission event generators, the CGMF and FREYA fission event generators both compute the decay of a large ensemble of fission fragments formed in excited states, following the emission of prompt neutrons and gamma rays sequentially and on an event-by-event basis. There are many differences between those codes that can explain differences observed in $P(\nu)$, but of particular importance is the distribution of fission fragments in total kinetic energy (TKE). While the average TKE correlates strongly with $\bar{\nu}$, the higher moments of the TKE distribution correlate strongly with the higher factorial moments of $P(\nu)$. However, other model parameters and assumptions that significantly differ between FREYA and CGMF can also explain discrepancies in this distribution.

5.2. Observables

Feynman histograms, singles rates R_1, doubles rates R_2, and leakage multiplication M_L are compared between the various codes for all BeRP-Ni and BeRP-W benchmark configurations. All results are calculated using a time width of $\tau = 1000\,\mu s$. It should be noted that because MCNP/CGMF requires significantly more computer time to reach the same statistical confidence as the other codes, and there were limitations on the available computer time, MCNP/CGMF results have much larger corresponding uncertainties.

5.2.1. BeRP-Ni configurations

Fig. 8 shows Feynman histograms for a few representative BeRP-Ni configurations. Appendix B contains Feynman histograms for all other BeRP-Ni configurations. All histograms are plotted on the same axes to make trends as a function of reflector thickness easier to observe. Measured results are also shown for comparison. Tables 4 present figure of merit (FOM) values, calculated according to Eq. (15) (Arthur et al., 2017), to quantify the discrepancy between the measured and various simulated Feynman histograms. In the FOM equation, N_{bins} represents total number of bins in the measured Feynman histogram being compared. M_i and S_i are the magnitudes of the ith bins of the measured and simulated histograms, respectively. $\sigma_{M,i}$ and $\sigma_{S,i}$ are the standard deviations corresponding to the ith measured and simulated bins. $|\frac{dM_L}{dC_i}|_{norm}$ is the normalized magnitude of the sensitivity of leakage multiplication to the ith bin in the measured Feynman histogram being compared. Because the sensitivity of leakage multiplication to each

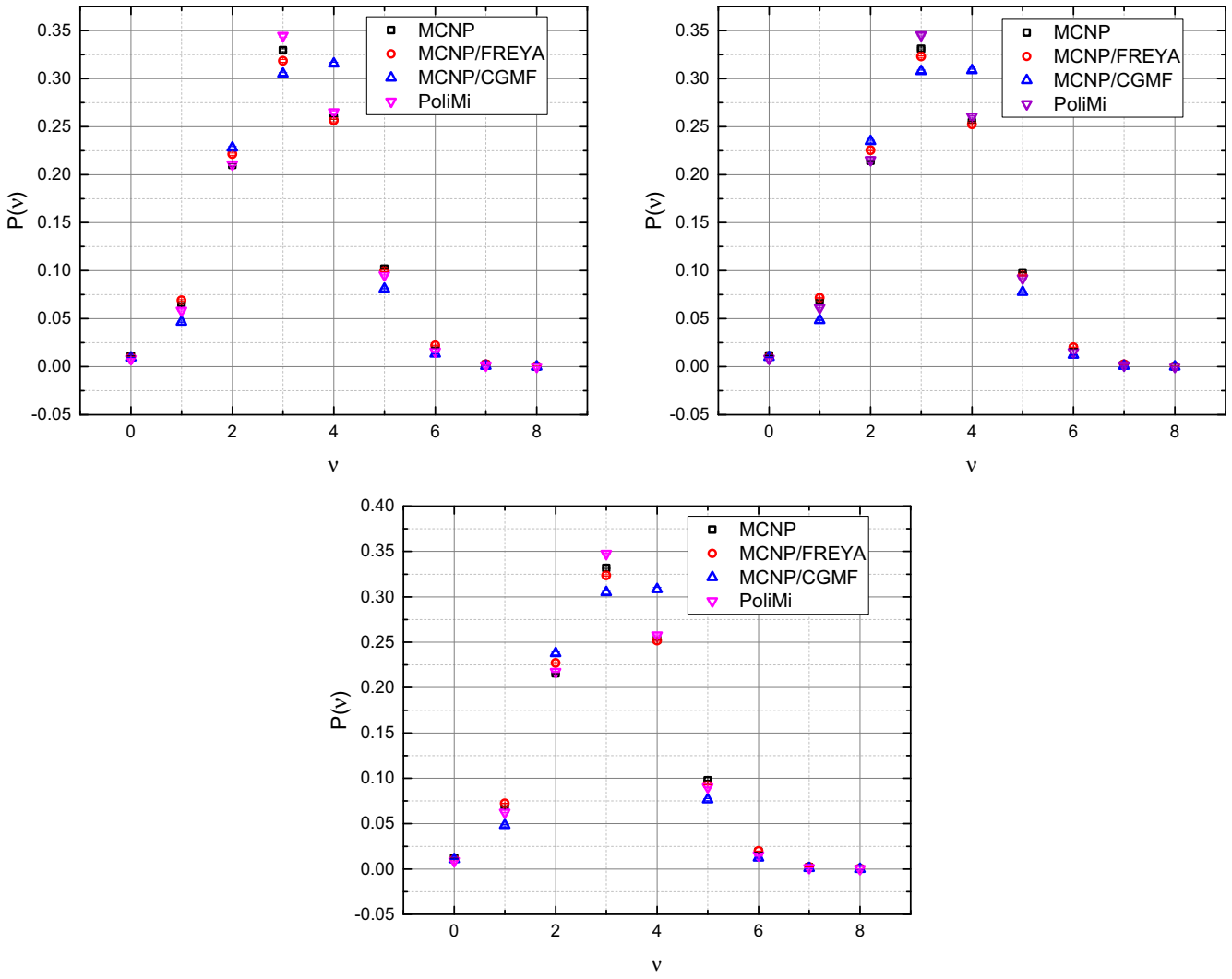

Fig. 7. ^{239}Pu induced fission multiplicity distributions for 0 (left), 1.5 (middle), and 3.0 (right) in. W thickness.

Table 3
^{239}Pu induced fission multiplicity distribution parameters for 0, 1.5, and 3.0 in. W thickness.

Code	$\bar{\nu}$	σ	$\bar{\nu}$	σ	$\bar{\nu}$	σ
W thickness (in.)	0	0	1.5	1.5	3.0	3.0
MCNP	3.16	1.43	3.13	1.43	3.12	1.43
MCNP/FREYA	3.15	1.47	3.12	1.45	3.10	1.44
MCNP/CGMF	3.17	1.25	3.14	1.24	3.14	1.25
PoliMi	3.16	1.31	3.13	1.31	3.12	1.31

bin in the histogram is included in the FOM equation, discrepancies between higher multiplet bins (which M_L is more sensitive to) affect the FOM more than discrepancies at multiplet bins that M_L is not very sensitive to. The ideal FOM value is unity.

$$FOM = \sum_{i=1}^{N_{bins}} \frac{(M_i - S_i)^2}{\sigma_{M,i}^2 + \sigma_{S,i}^2} \left| \frac{dM_L}{dC_i} \right|_{norm} \tag{15}$$

From the tabulated FOM values, which Fig. 9 shows in plot form, it is clear that according to this metric MCNP/CGMF performs the best for almost all nickel thicknesses (for the 1 in. reflected configuration MCNP/CGMF shows slightly worse performance than PoliMi). PoliMi shows the next best performance, followed by MCNP. Finally, MCNP/FREYA shows the worst performance according to this FOM, especially at smaller (0–1.5 in.) reflector thicknesses. The MCNP/FREYA FOM values show a clear downward trend between 0.5 and 2.0 in. nickel thickness. However, it should be noted that it is not technically correct to compare the FOM values for MCNP/CGMF Feynman histograms to the FOM values corresponding to the other codes. As can be determined from Eq. (15), the FOM values are affected by the magnitude of the uncertainties. Therefore, accurate comparisons between FOM values can only truly be made between histograms that have similar uncertainties. The uncertainties corresponding to MCNP/CGMF histograms, especially at large reflector thicknesses, are up to an order of magnitude larger than those corresponding to the other codes. This is why Fig. 8 clearly shows that MCNP/CGMF data do not compare to the measured data as well as the other codes, yet the FOM value in Table 4 indicates very good matching of experimental data, as compared to the other codes.

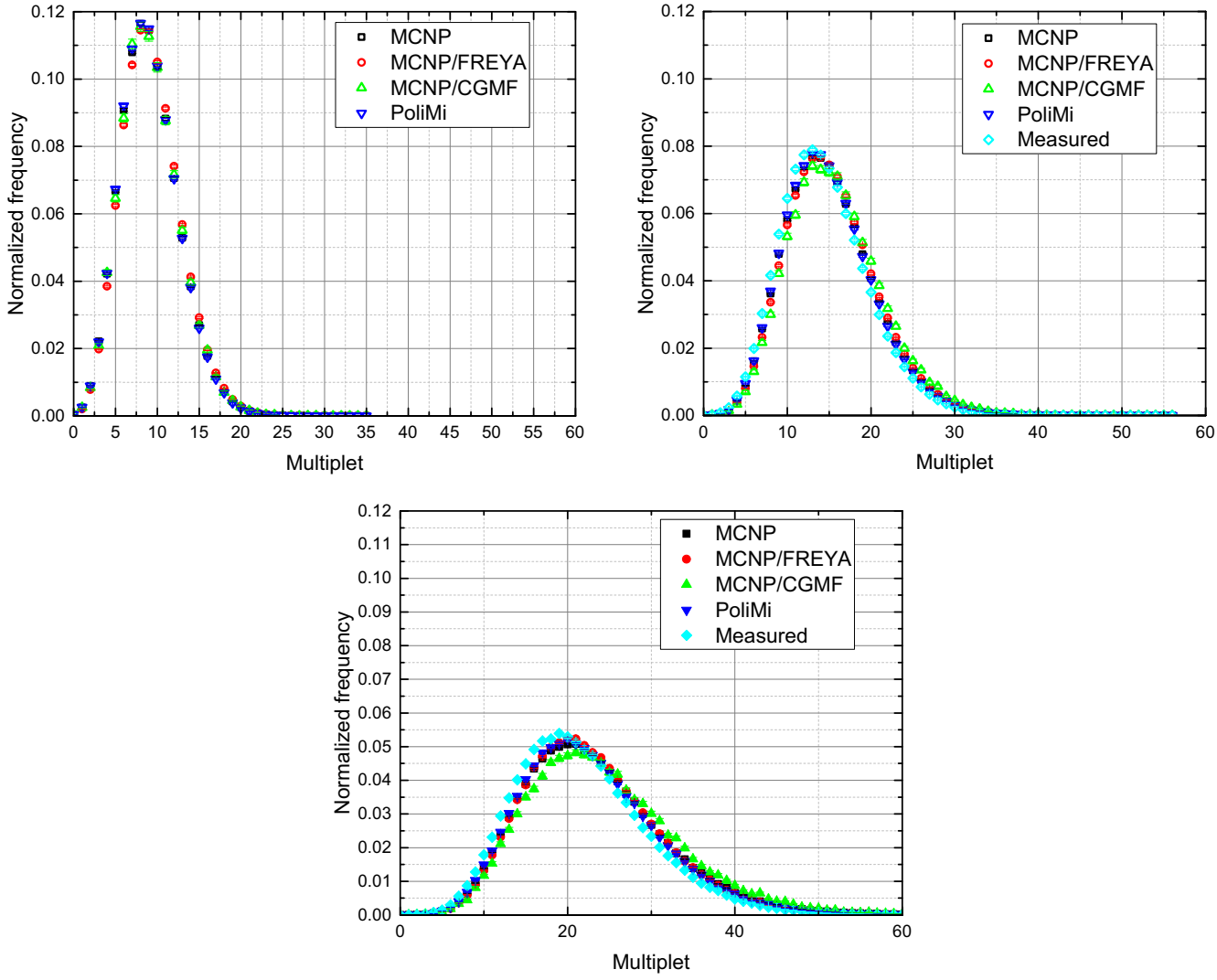

Fig. 8. Feynman histograms for 0 (left), 1.5 (middle), and 3.0 (right) in. Ni thickness.

Table 4
FOM values for the various simulated Feynman histograms, as compared to the measured histogram, for 0, 1.5, and 3.0 in. Ni thickness.

Code	0 in. Ni thickness	1.5 in. Ni thickness	3.0 in. Ni thickness
MCNP	24	39	38
MCNP/FREYA	82	55	32
MCNP/CGMF	5.9	24	24
PoliMi	19	25	24

Figs. 10 and 11 are plots of singles and doubles rates.

Overall, PoliMi seems to show the best match to experimental singles and doubles results, while MCNP/CGMF shows the most deviation from experimental results. MCNP performance seems to worsen as a function of nickel thickness, while MCNP/FREYA shows the opposite trend.

Fig. 12 plots leakage multiplication for the various BeRP-Ni configurations.

Unlike with singles and doubles rates, MCNP shows the best agreement with leakage multiplication. PoliMi shows a consistent under-bias, while MCNP/CGMF shows a consistent over-bias.

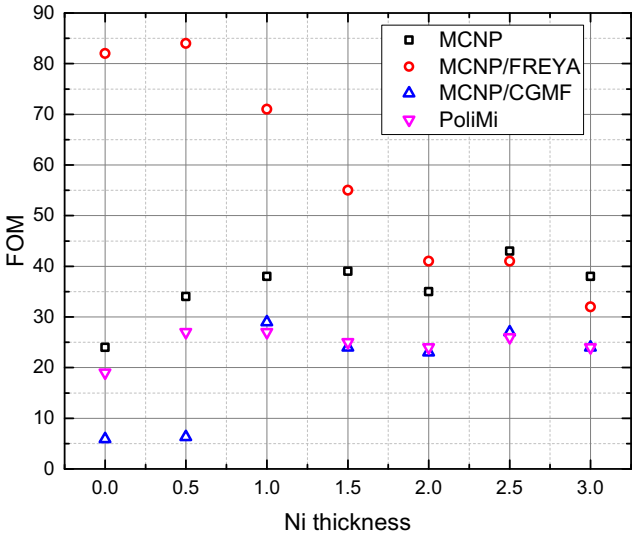

Fig. 9. Feynman histogram FOM values for all codes and all Ni thicknesses.

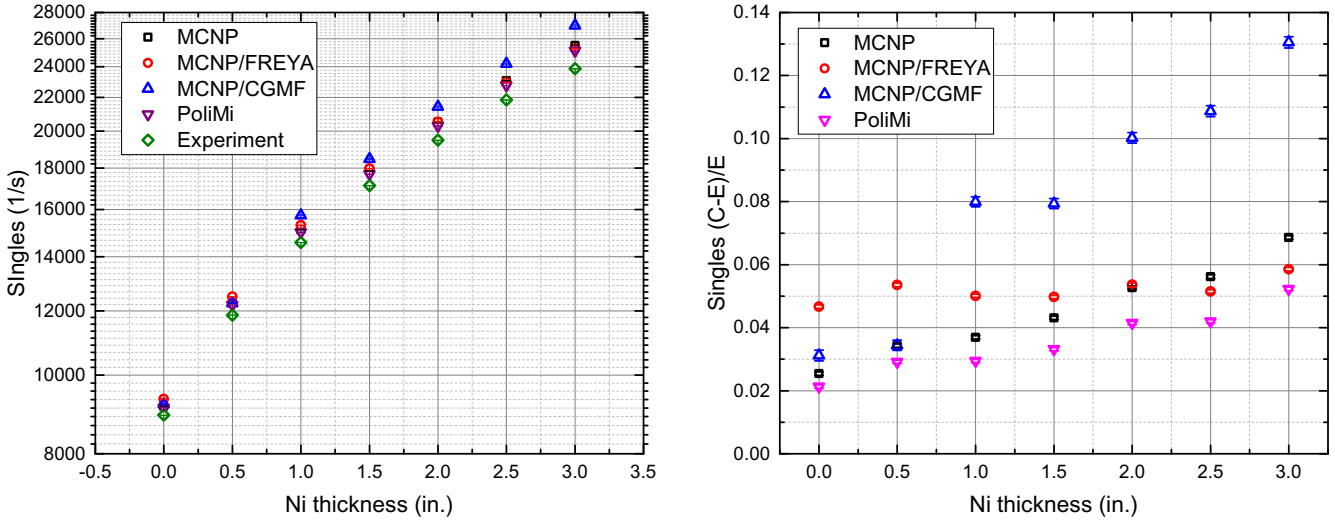

Fig. 10. Singles rates for all BeRP-Ni configurations.

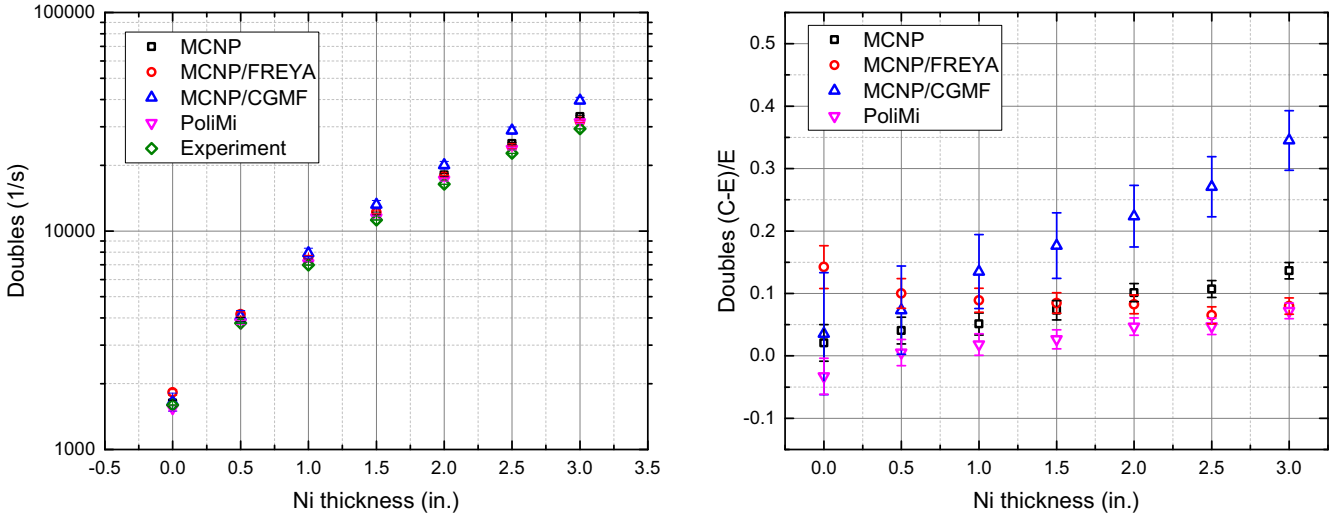

Fig. 11. Doubles rates for all BeRP-Ni configurations.

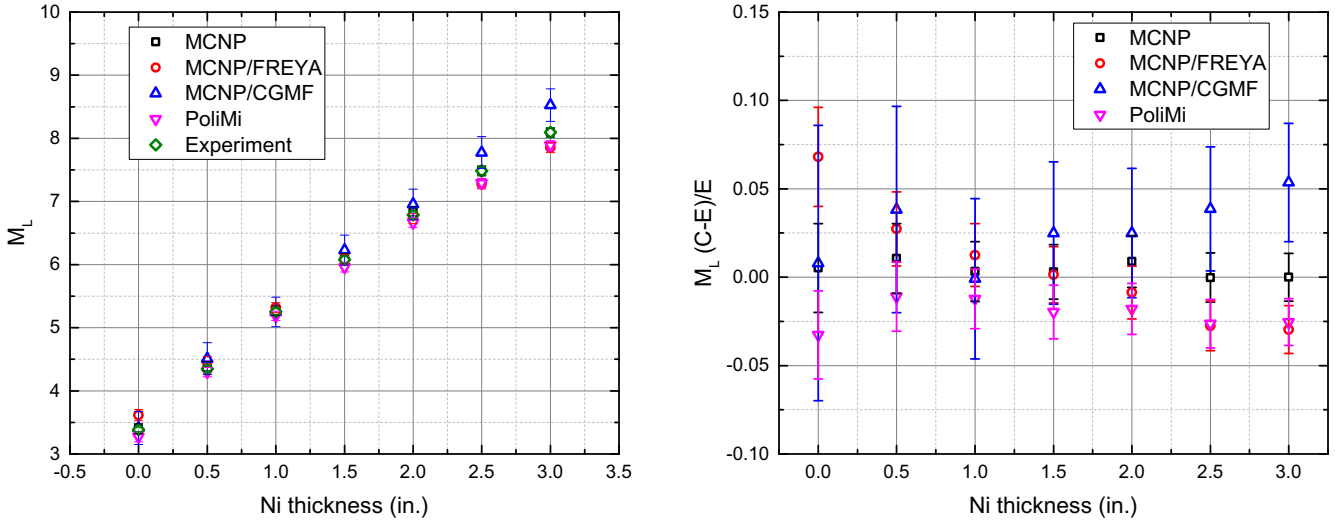

Fig. 12. Leakage multiplication for all BeRP-Ni configurations.

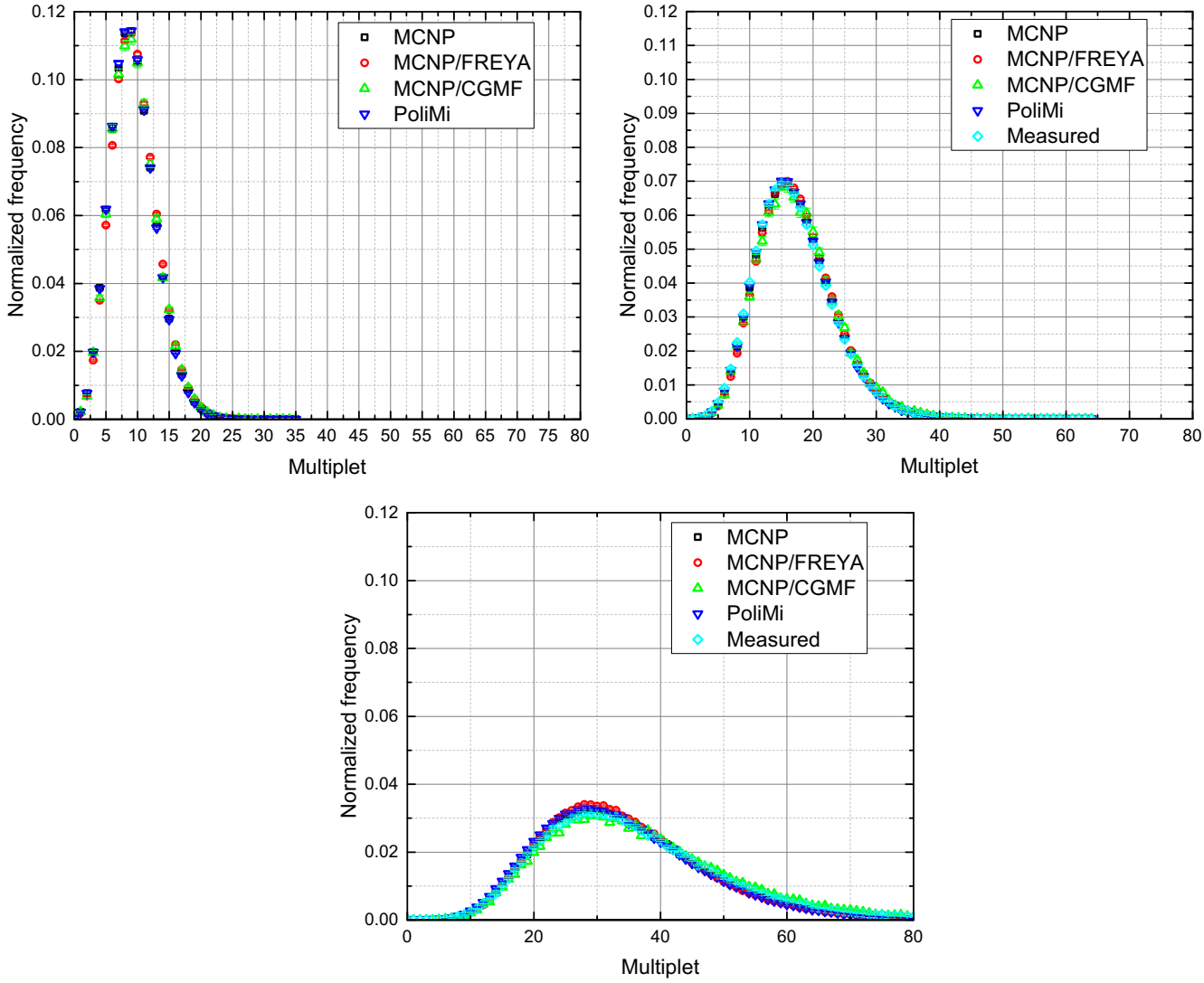

Fig. 13. Feynman histograms for 0 (left), 1.5 (middle), and 3.0 (right) in. W thickness.

MCNP/FREYA performance seems to improve with increasing nickel thickness, and then begin to worsen again after 1.5 in. of nickel reflection.

5.2.2. BeRP-W configurations

Fig. 13 shows Feynman histograms for a few representative BeRP-W configurations. Appendix B contains Feynman histograms for all other BeRP-W configurations. All histograms are plotted on the same axes to make trends as a function of reflector thickness easier to observe. Measured results are also shown for comparison. Table 5 presents FOM values to quantify the discrepancy between the measured and various simulated Feynman histograms.

Table 5
FOM values for the various simulated Feynman histograms, as compared to the measured histogram, for 0, 1.5, and 3.0 in. W thickness.

Code	0 in. W thickness	1.5 in. W thickness	3.0 in. W thickness
MCNP	88	1.8	1.1
MCNP/FREYA	$1.9 * 10^2$	4.9	5.8
MCNP/CGMF	19	3.0	2.5
PoliMi	78	1.8	4.8

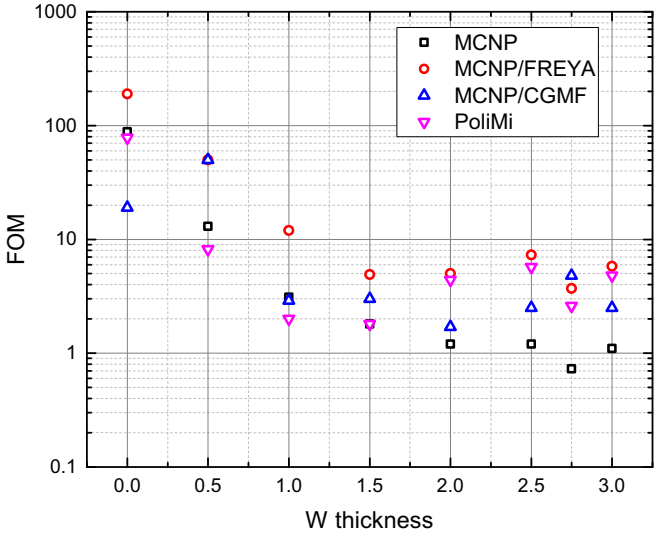

Fig. 14. Feynman histogram FOM values for all codes and all W thicknesses.

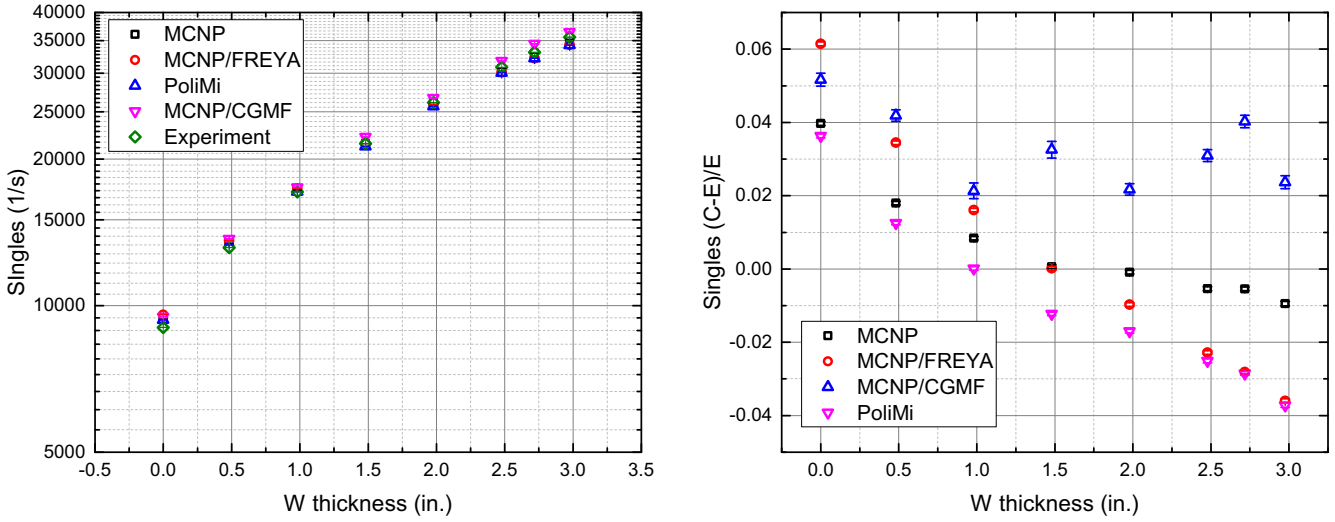

Fig. 15. Singles rates for all BeRP-W configurations.

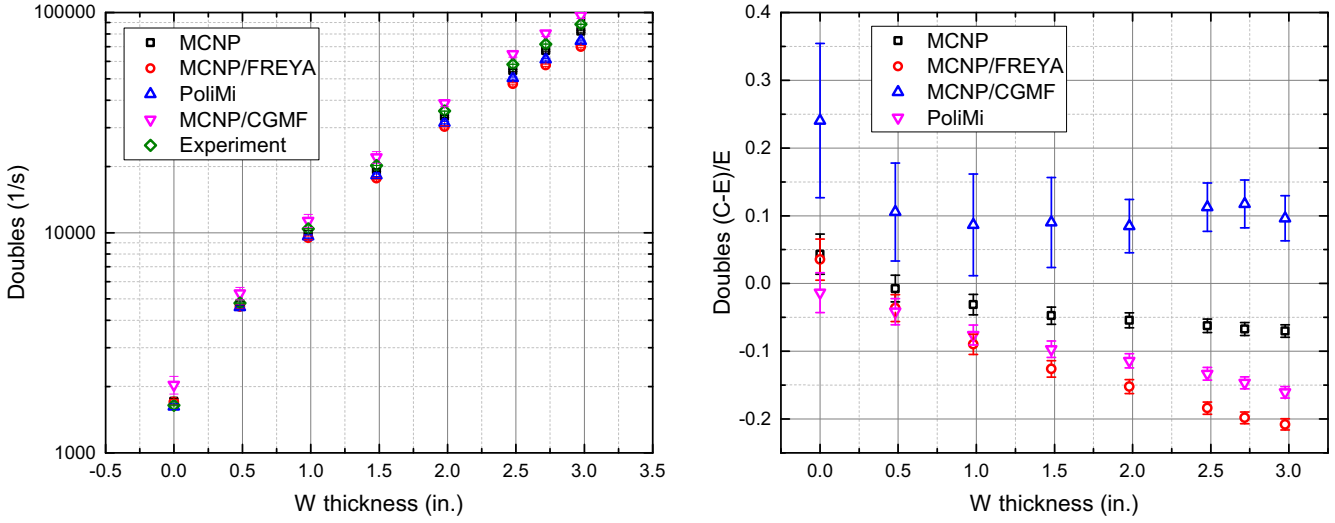

Fig. 16. Doubles rates for all BeRP-W configurations.

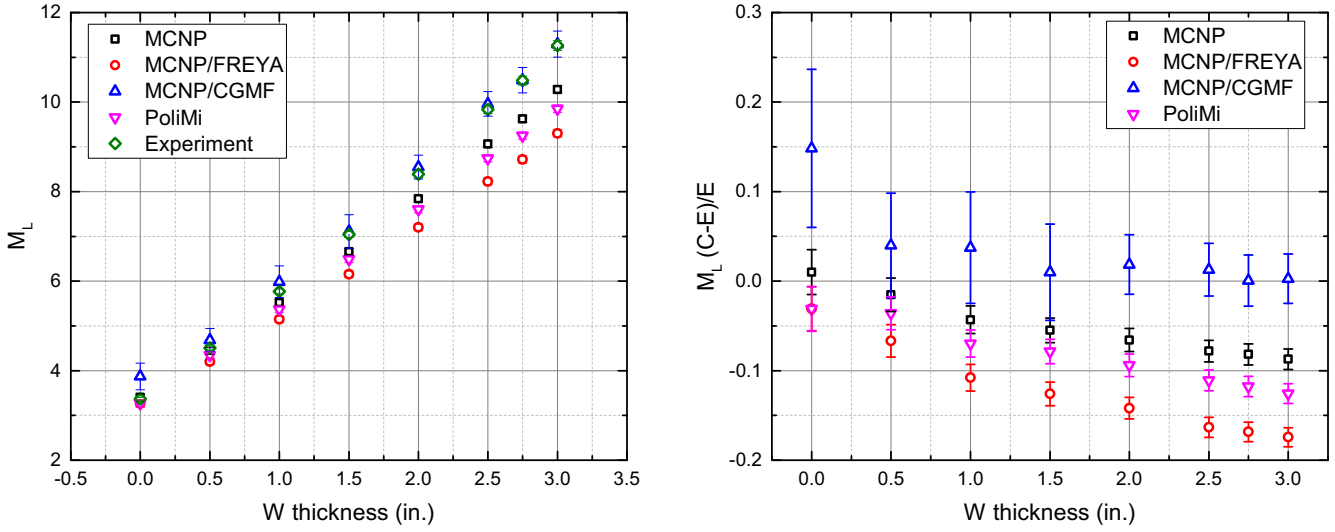

Fig. 17. Leakage multiplication for all BeRP-W configurations.

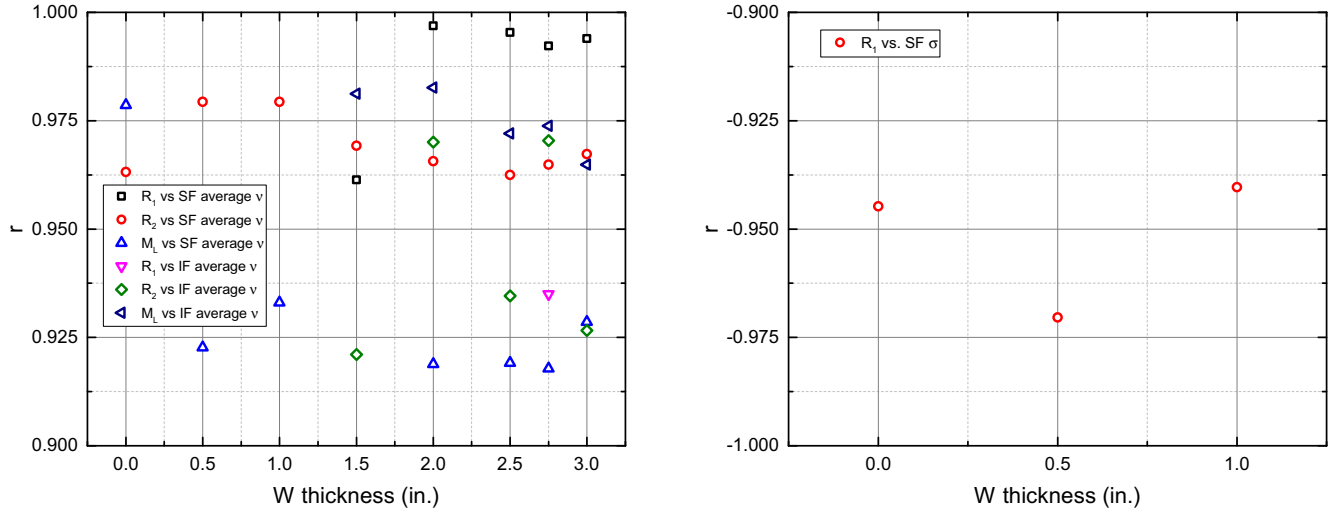

Fig. 18. Pearson correlation coefficient "r" plotted for the most highly correlated combinations of observables and nuclear data items of interest, across all configurations of the BeRP-W benchmark.

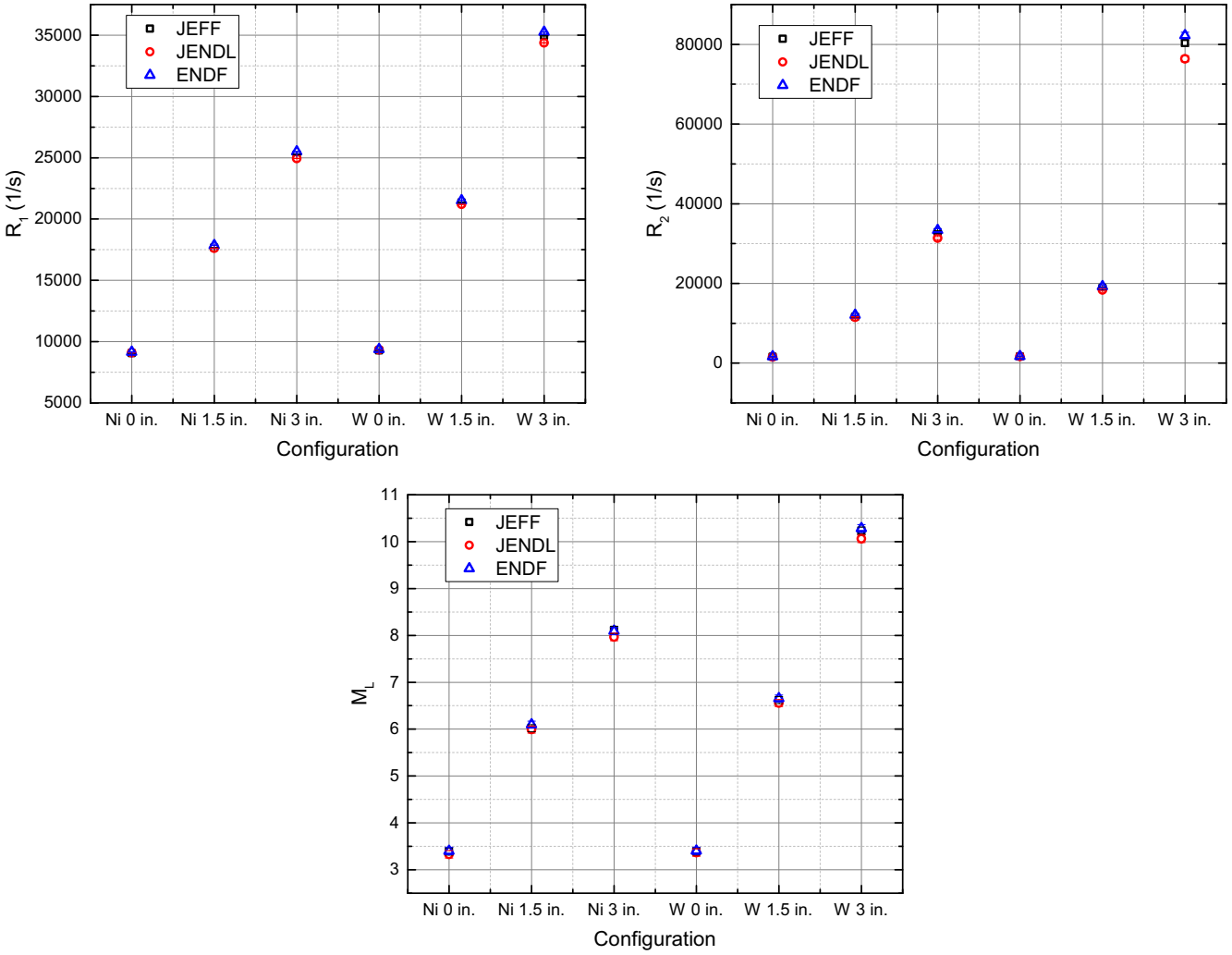

Fig. 19. BeRP-Ni and BeRP-W maximum (3 in.), middling (1.5 in.), and minimum (0 in.) reflected configurations, run with ^{239}Pu and ^{240}Pu nuclear data taken from JEFF-3.2 and JENDL-4.0, as compared to ENDF/B-VII.1.

Except for the poorer code performance for the small reflector thickness configurations, the tabulated FOM values, which Fig. 14 shows in plot form, are quite good (<10) and very close together. For 1.5-3 in. W reflector thickness, MCNP shows the best performance, followed by PoliMi for 1.5-2 in. W thickness and MCNP/CGMF for 2.5-3 in. W thickness. MCNP/FREYA shows the worst performance, according to this FOM, for all configurations.

Figs. 15 and 16 are plots of singles and doubles rates.

MCNP seems to show the best agreement with measured singles and doubles rates for cases with thick tungsten reflection. MCNP/CGMF is the most discrepant from measured singles rates, but similar in deviation from experiment to both PoliMi and MCNP/FREYA for doubles rates. MCNP/CGMF has a consistent over-bias in both singles and doubles rates, while PoliMi and MCNP/FREYA show consistent under-biases in doubles rates.

Fig. 17 plots leakage multiplication for the various BeRP-W configurations.

MCNP/CGMF shows the best agreement with experimental leakage multiplication data. MCNP shows the next best agreement, followed by PoliMi, and then MCNP/FREYA. MCNP, PoliMi, and MCNP/FREYA all show significant under-bias for predicting interred leakage multiplication.

5.2.3. Correlations with nuclear data

Correlations are observed to exist between differences in the multiplicity distribution nuclear data (induced and spontaneous fission $\bar{\nu}$ and σ) used by or extracted from the various codes, and differences in observables of interest (R_1, R_2, and M_L). As previously mentioned, 96 Pearson correlation coefficients exist over all configurations of the BeRP-W benchmark. These are plotted in Appendix C. The coefficients showing the largest correlations (defined as a correlation or anti-correlation value above 90%) are plotted in Fig. 18.

The strongest correlations are between R_1, R_2, and M_L, and both SF and IF $\bar{\nu}$, especially for the highly reflected configurations. The strongest anti-correlations are between R_1 and SF σ, for the less reflected configurations. The observed correlations between multiplicity distribution nuclear data and observables of interest may aid in future subcritical benchmark experiment design, by allowing experimenters to focus on observables that seem most sensitive to the nuclear data quantity of interest.

5.2.4. Other nuclear data libraries

The minimum, middling, and maximum reflected cases of the BeRP-Ni and BeRP-W benchmarks were run with MCNP, with the ENDF/B-VII.1 nuclear data for ^{239}Pu and ^{240}Pu replaced by JEFF-3.2 nuclear data, and JENDL-4.0 nuclear data. Fig. 19 shows the results. Fig. 20 plots comparisons to experimental results.

The results from the three nuclear data libraries (ENDF, JEFF, and JENDL) do show some variation, which should be investigated further. It should be noted that the significant worsening in leakage multiplication (C-E)/E value for configuration 7 of the BeRP-W benchmark is not unexpected. As the trend in Fig. 17 shows,

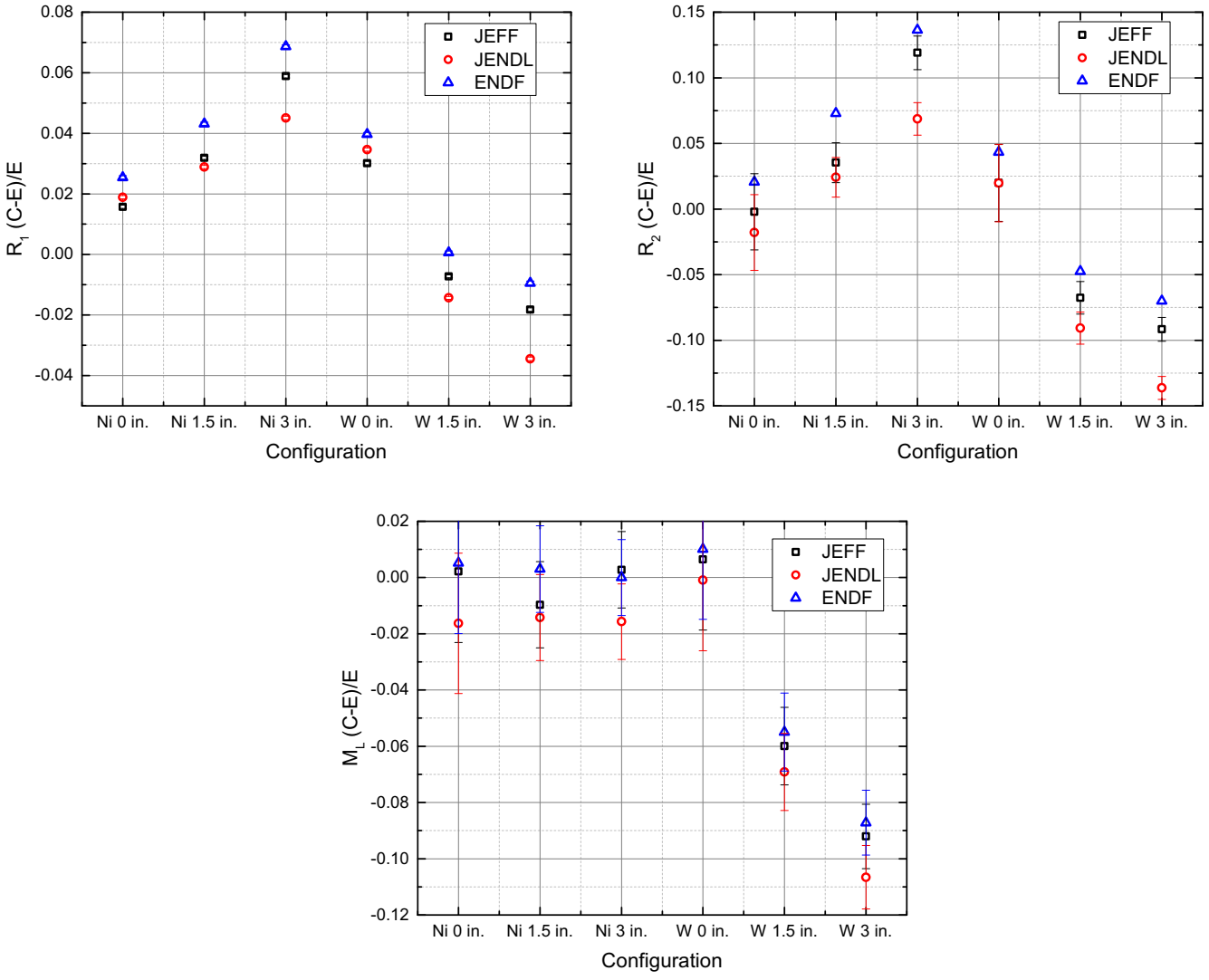

Fig. 20. BeRP-Ni and BeRP-W maximum (3 in.), middling (1.5 in.), and minimum (0 in.) reflected configurations, run with ^{239}Pu and ^{240}Pu nuclear data taken from JEFF-3.2 and JENDL-4.0, as compared to ENDF/B-VII.1.

simulated leakage multiplication values often compare less well as reflection, and therefore leakage multiplication itself, increases.

6. Conclusions

This work established a method to compare codes that take into account the correlated physics of fission. As more subcritical benchmark configurations become available, this method will continue to be utilized to help in code comparison. The results of this work clearly show that there is currently no best performer among the various radiation transport codes investigated here. In fact, based on the current status of these codes, there does not seem to be much reason to use the more computationally intensive fission event generator codes (MCNP/FREYA and MCNP/CGMF) over the others, for the specific application of subcritical neutron multiplication inference benchmarks. Due to the fact that the MC codes investigated in this work show different discrepancies for different measured configurations and different correlated neutron observables, it is difficult to determine which codes show best overall performance in this area. In addition, the CGMF and FREYA fission event generators are fairly recent capabilities that are still part of ongoing work for validation and improvements, and this work is part of a collaboration with the individuals currently implementing CGMF and FREYA in MCNP. Because of this continuing development process, the fission event generators are still changing with time and it is difficult to truly dive into the physical effects at this time.

If better performance is defined as less deviation from measured results, MCNP/CGMF and MCNP perform best for BeRP-Ni and BeRP-W Feynman histogram results, respectively. PoliMi performs best for BeRP-Ni singles and doubles rates. However, MCNP performs best for BeRP-Ni leakage multiplication. MCNP performs best for BeRP-W singles and doubles rates, while MCNP/CGMF performs better for BeRP-W leakage multiplication. One disadvantage to the plutonium measurements is that all of the observables are linked to both induced and spontaneous fission. In the future it would be interesting to look at a passive high-enriched uranium system(s) in which only induced fission plays a significant role (with the downside of worsened statistics), and possibly other uranium system measurements as well (Arthur et al., 2018; Hutchinson et al., 2013; Hutchinson et al., 2012; Hutchinson et al., 2014; Chapelle et al., 2014). More investigation is necessary to determine which codes truly perform better in which areas, and how such information can be used to improve simulation capabilities overall. However, it is clear that the MC radiation transport codes used in this work do not show adequate agreement to measured data. Especially for the fields of safeguards and criticality safety, even better agreement is desired (Trahan et al., 2016; Hutchinson et al., 2016). As more subcritical benchmark configurations become available, this method will continue to be utilized to help in code comparison.

Although it is difficult to determine which radiation transport code shows the best overall performance in simulating subcritical neutron multiplication inference benchmark measurements, it is clear that correlations exist between the underlying nuclear data utilized by (or generated by) the various codes, and the correlated neutron observables of interest. According to the Pearson correlation coefficient, strong (r>0.90) correlations exist between R_1, R_2, and M_L, and both SF and IF $\bar{\nu}$, especially for the highly reflected configurations of the BeRP-W benchmark. Strong (r<-0.90) anti-correlations exist between R_1 and SFσ for the less reflected configurations.. This could prove useful in nuclear data validation and evaluation applications, in which a particular moment of the neutron mulitplicity distribution is of more interest than the other moments. In addition, interesting trends of performance versus metal reflector thickness have been observed, which trends differ between codes. It would be very beneficial to investigate what aspects of each code cause these trends in performance quality. Finally, the variations in observables of interest caused by replacing ENDF/B-VII.1 ^{239}Pu and ^{240}Pu nuclear data with JEFF-3.2 and JENDL-4.0 nuclear data should be investigated further. The types of comparisons investigated in this work will become even more important as additional subcritical benchmark configurations are published as it may then be easier to distinguish which codes and nuclear data evaluations perform the best for the measured observables.

Acknowledgments

This material is based upon work supported in part by the Department of Energy National Nuclear Security Administration under Award Number(s) DE-NA0002576. This work was also supported in part by the DOE Nuclear Criticality Safety Program, funded and managed by the National Nuclear Security Administration for the Department of Energy.

Appendix A

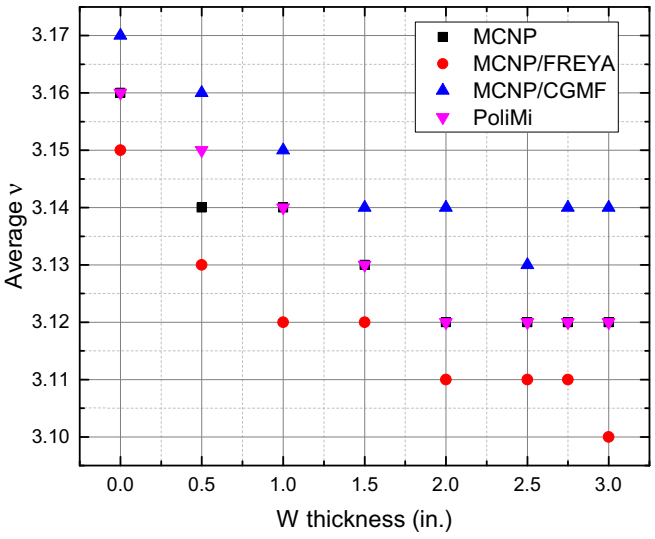

Fig. 21. ^{239}Pu induced fission $\bar{\nu}$ as a function of W thickness.

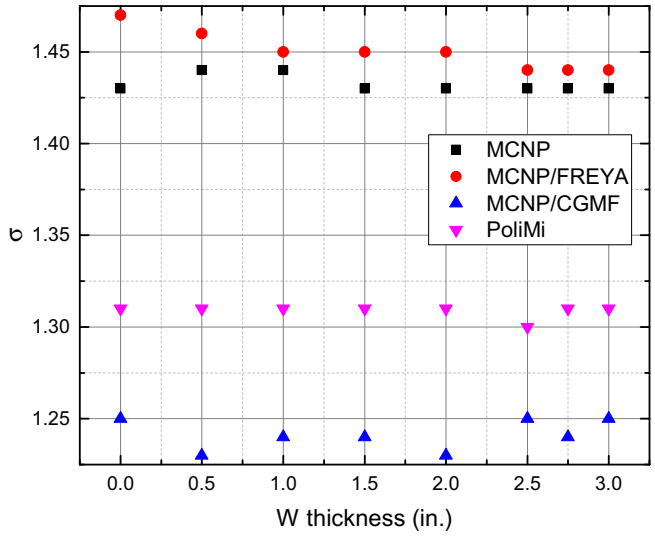

Fig. 22. ^{239}Pu induced fission σ as a function of W thickness.

Appendix B

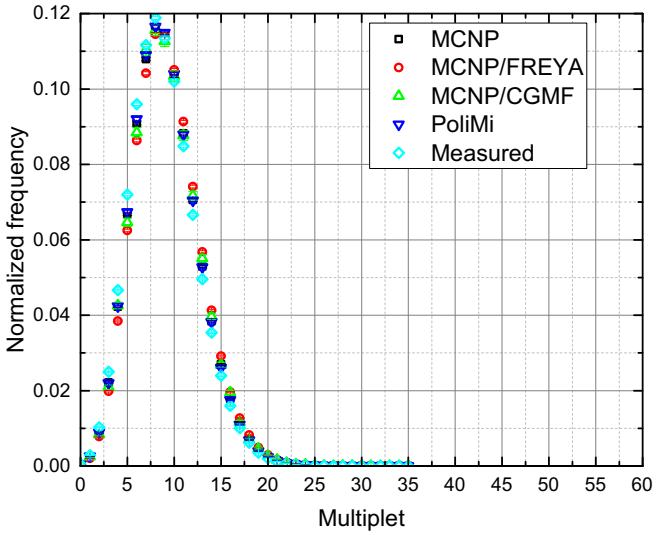

Fig. 23. Feynman histograms for 0.5 in. Ni thickness.

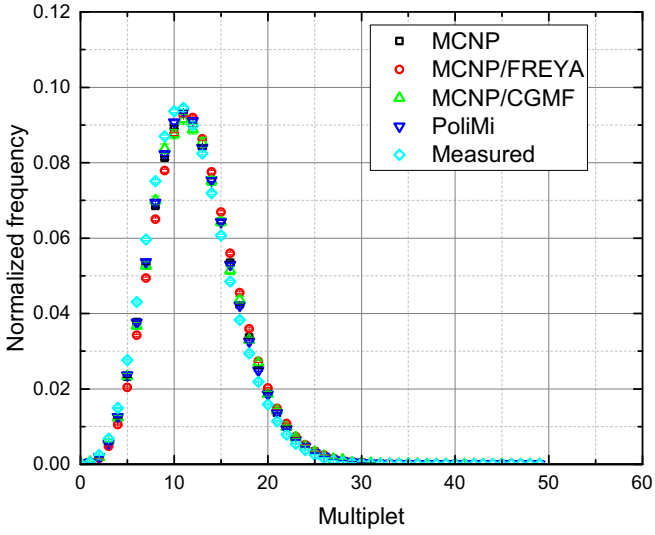

Fig. 24. Feynman histograms for 1 in. Ni thickness.

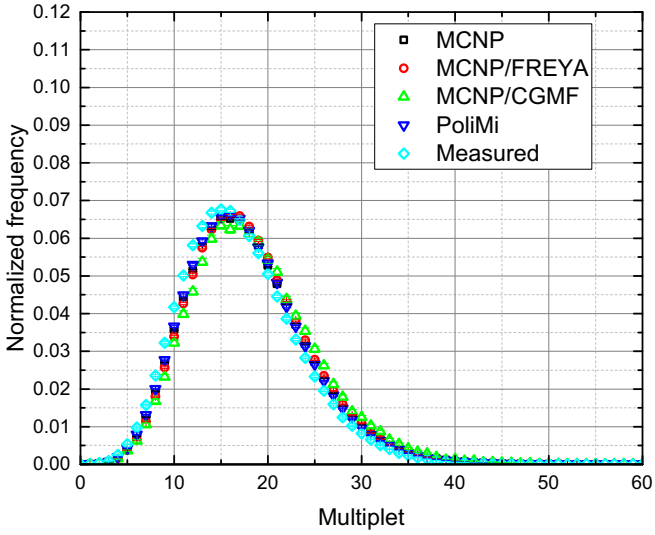

Fig. 25. Feynman histograms for 2 in. Ni thickness.

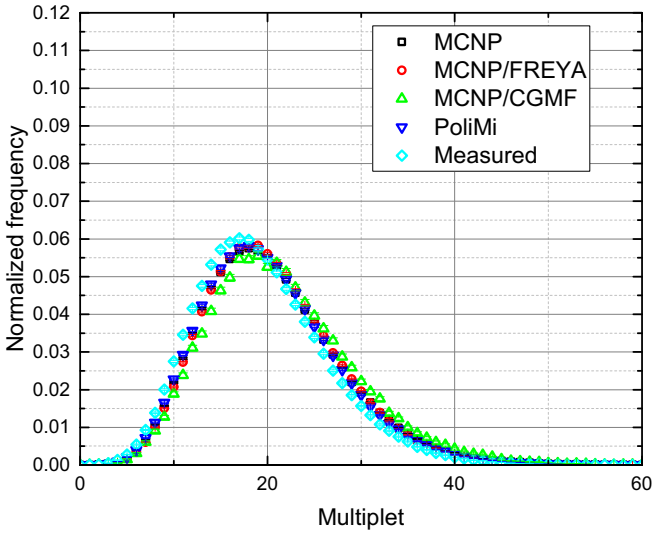

Fig. 26. Feynman histograms for 2.5 in. Ni thickness.

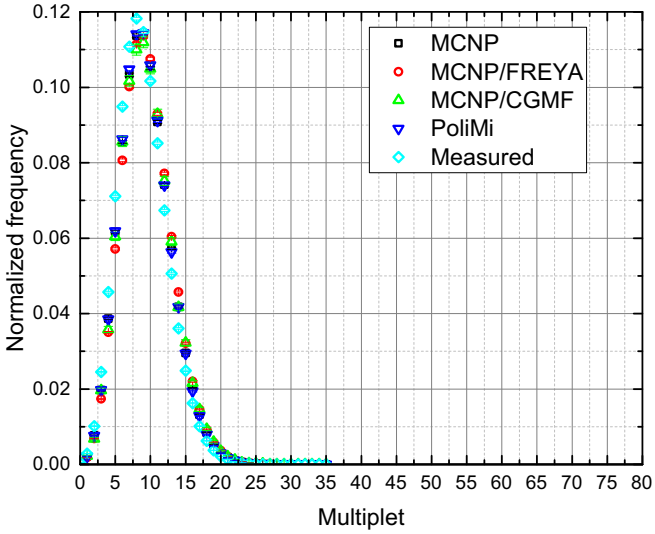

Fig. 27. Feynman histograms for 0.5 in. W thickness.

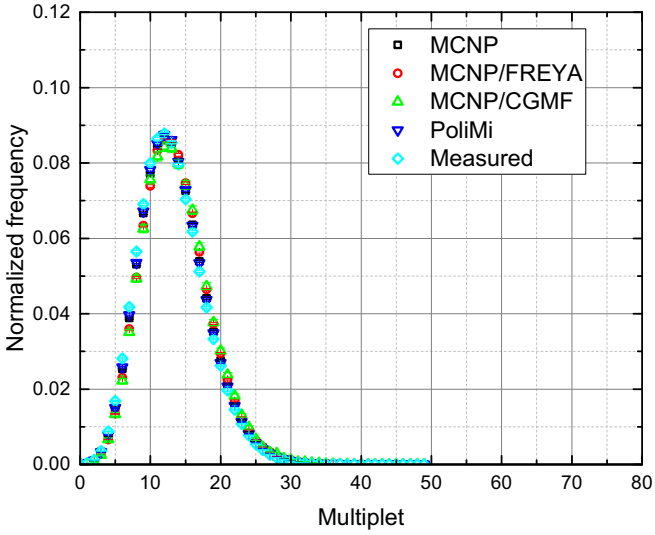

Fig. 28. Feynman histograms for 1 in. W thickness.

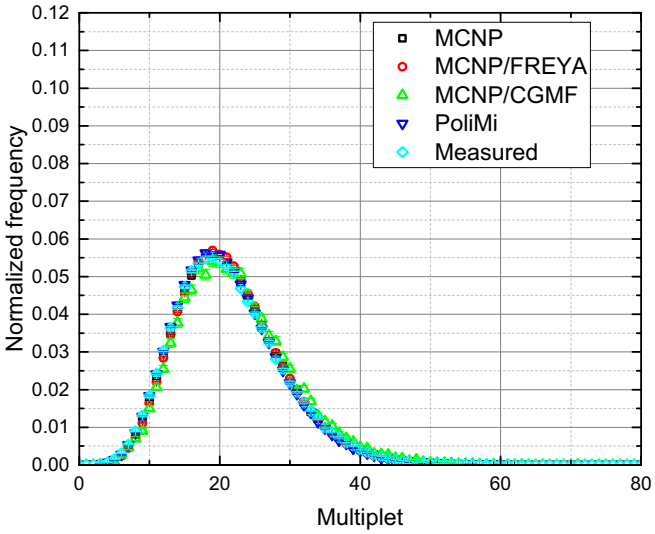

Fig. 29. Feynman histograms for 2 in. W thickness.

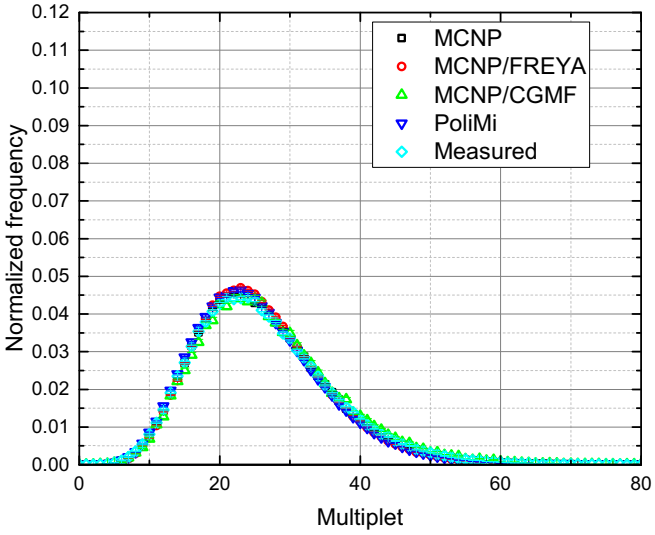

Fig. 30. Feynman histograms for 2.5 in. W thickness.

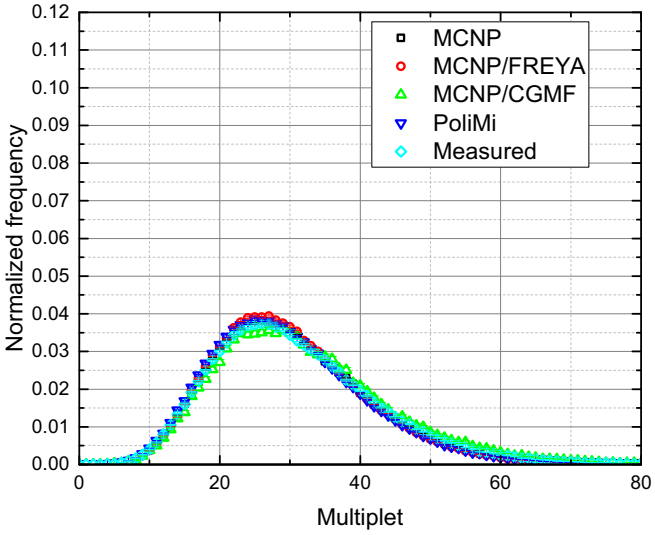

Fig. 31. Feynman histograms for 2.75 in. W thickness.

Table 6
FOM values for the various simulated Feynman histograms, as compared to the measured histogram, for 0.5, 1.0, 2.0, and 2.5 in. Ni thickness.

Code	0.5 in. Ni thickness	1.0 in. Ni thickness	2.0 in. Ni thickness	2.5 in. Ni thickness
MCNP	34	38	35	43
MCNP/FREYA	84	71	41	41
MCNP/CGMF	6.3	29	23	27
PoliMi	27	27	24	26

Table 7
FOM values for the various simulated Feynman histograms, as compared to the measured histogram, for 0.5, 1.0, 2.0, 2.5, and 2.75 in. W thickness.

Code	0.5 in. W thickness	1.0 in. W hickness	2.0 in. W thickness	2.5 in. W thickness	2.75 in. W thickness
MCNP	13	3.1	1.2	1.2	0.73
MCNP/FREYA	50	12	5.0	7.3	3.7
MCNP/CGMF	50	2.9	1.7	2.5	4.8
PoliMi	8.2	2.0	4.4	5.7	2.6

Appendix C

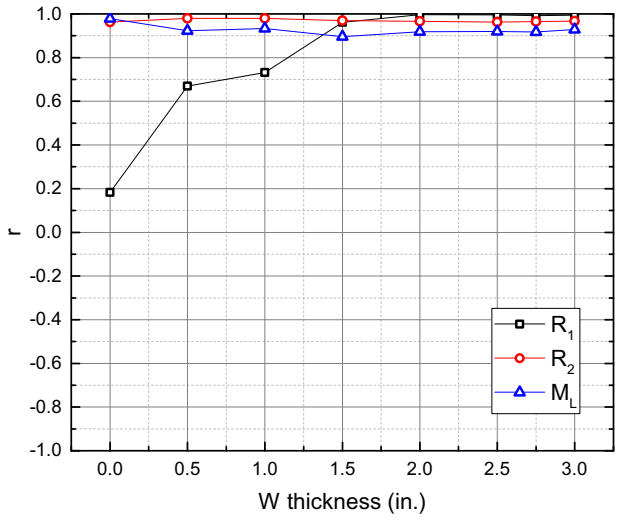

Fig. 32. Pearson correlation coefficient "r" plotted for all observables of interest vs. SF $\bar{\nu}$, across all configurations of the BeRP-W benchmark.

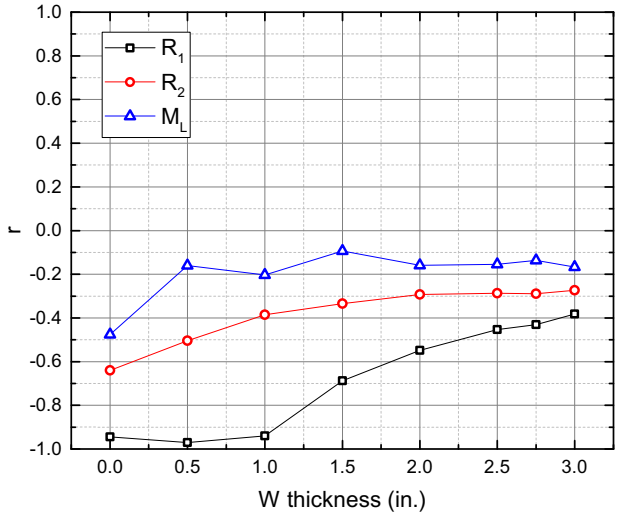

Fig. 33. Pearson correlation coefficient "r" plotted for all observables of interest vs. SF σ, across all configurations of the BeRP-W benchmark.

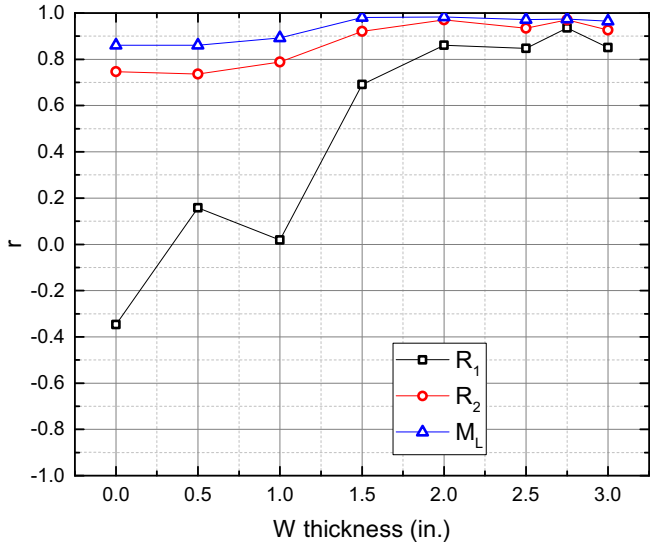

Fig. 34. Pearson correlation coefficient "r" plotted for all observables of interest vs. IF $\bar{\nu}$, across all configurations of the BeRP-W benchmark.

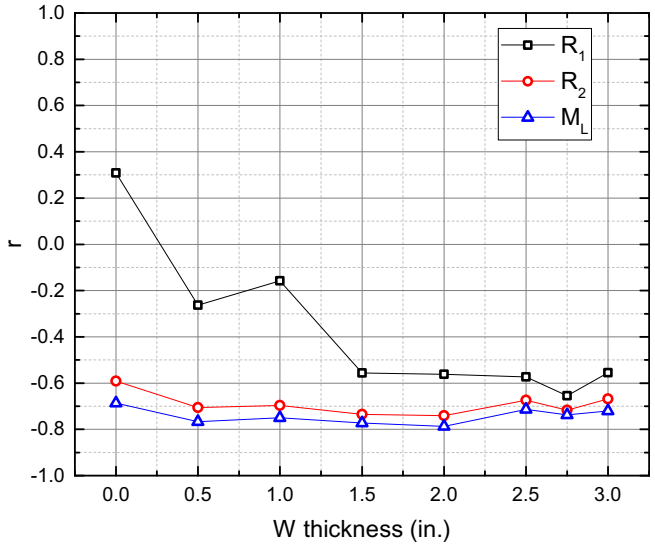

Fig. 35. Pearson correlation coefficient "r" plotted for all observables of interest vs. IF σ, across all configurations of the BeRP-W benchmark.

References

Arthur, J.A., Bahran, R.M., Hutchinson, J.D., Rising, M.E., Pozzi, S.A., 2016. Comparison of the performance of various correlated fission multiplicity monte carlo codes. In: Transactions of the American Nuclear Society Winter Meeting and Technology Expo.

Arthur, J., Bahran, R., Hutchinson, J., Grove, T., Pozzi, S., 2017. Improved figure of merit for feynman histograms. In: Transactions of the American Nuclear Society Winter Meeting and Technology Expo.

Arthur, J., Bahran, R., Hutchinson, J., Sood, A., Thompson, N., Pozzi, S., 2018. Development of a research reactor protocol for neutron multiplication measurements. Prog. Nucl. Energy 106, 120–139.

Bahran, R., Hutchinson, J., 2016. Subcritical copper-reflected α-phase plutonium (SCRαP) integral experiment design. Trans. Am. Nucl. Soc. 114, 527–529.

Bahran, R., Hutchinson, J., Richard, B., Sood, A., 2014. List-mode simulations of the Thor core benchmark sensitivity experiments. Transactions of the American Nuclear Society Annual Meeting, vol. 111, pp. 805–808.

Bahran, R., Croft, S., Hutchinson, J., Smith, M., Sood, A., 2014. A survey of nuclear data deficiences affecting nuclear non-proliferation. In: Proceedings of the 2014 INMM Annual Meeting, Atlanta GA.

Barnard, E., Ferguson, A., McMurray, W., Heerden, I.V., 1965. Time-of-flight measurements of neutron spectra from the fission of U^{235}, U^{238}, and Pu^{239}. Nucl. Phys. 71, 228–249.

Boldeman, J.W., Hines, M.G., 1985. Prompt neutron emission probabilities following spontaneous and thermal neutron fission. Nucl. Sci. Eng. 91, 114–116.

Bolding, S.R., Solomon, C.J., 2013. Simulations of multiplicity distributions with perturbations to nuclear data. Trans. Am. Nucl. Soc. 109, 251–254.

Briggs, J.B., 2003. The international criticality safety benchmark evaluation project (ICSBEP). In: International Conference on Nuclear Energy for New Europe.

Briggs, J. et al., 2014. Integral benchmark data for nuclear data testing through the ICSBEP & IRPhEP. Nucl. Data Sheets 118, 396–400.

Chadwick, M. et al., 2006. ENDF/B-VII.0: next generation evaluated nuclear data library for nuclear science and technology. Nucl. Data Sheets 107, 2931–3060.

Chadwick, M. et al., 2011. ENDF/B-VII.1 nuclear data for science and technology: cross sections, covariances, fission product yields and decay data. Nucl. Data Sheets 112, 2887–2996.

Chapelle, A., Casoli, P., Authier, N., Myers, W., Hutchinson, J., Sood, A., Rooney, B., 2014. Joint neutron noise measurements on metallic reactor caliban. Nucl. Data Sheets 118, 558–560.

Cifarelli, D., Hage, W., 1986. Models for a three-parameter analysis of neutron signal correlation measurements for fissile material assay. Nucl. Instrum. Methods A251, 550–563.

Flerov, N.N., Talyzin, V.M., 1960. Average numbers ν and η of neutrons in the fission of ^{233}U and ^{239}Pu by 14 MeV neutrons. Transl. Atomnaya Energiya 10, 68–69.

Goorely, J. et al., 2012. Initial MCNP6 release overview. Nucl. Technol. 180, 298–315.

Hagmann, C. et al., 2013. FREYA-A new monte carlo code for improved modeling of fission chains. IEEE Trans. Nucl. Sci. 60, 545–549.

Hauser, W., Feshbach, H., 1952. The inelastic scattering of neutrons. Phys. Rev. 87.

Holden, N.E., Zucker, M.S., 1988. Prompt neutron emission multiplicity distribution and average values (nubar) at 200 m/s for the fissile nuclides. Nucl. Sci. Eng. 98 (2), 174–181.

Howerton, R., 1977. Nucl. Sci. Eng. 62, 438–454 (Revisited).

Hutchinson, J., Loaiza, D., 2007. Plutonium sphere reflected by beryllium. In: International Handbook of Evaluated Criticality Safety Benchmark Experiments, NEA/NSC/DOC/(95)03/I, PU-MET-FAST-038.

Hutchinson, J., Sood, A., Myers, W., Smith-Nelson, M., Dinwiddie, D., 2012. Comparison of heu measurements using measured and simulated data. Trans. Am. Nucl. Soc.

Hutchinson, J., Rooney, B., Myers, W., Sood, A., Smith-Nelson, M., 2013. CALIBAN measurements near delayed critical using subcritical measurement methods. In: 2013 American Nuclear Society Winter Meeting, Washington DC.

Hutchinson, J., Sood, A., Myers, W., Smith-Nelson, M., Dinwiddie, D., 2013. Comparison of HEU measurements using measured and simulated data. Trans. Am. Nucl. Soc. 106, 487–489.

Hutchinson, J., Rooney, B., Myers, W., Sood, A., Smith-Nelson, M., 2013. Caliban measurements near delayed critical using subcritical measurement methods. In: Transactions of the American Nuclear Society Winter Meeting and Technology Expo.

Hutchinson, J., Smith-Nelson, M.A., Sood, A., Goda, J.M., Bounds, J.A., 2014. Joint LANL/CEA measurements on Godiva IV. In: 2014 American Nuclear Society Annual Meeting, Reno NV.

Hutchinson, J., Nelson, M.A., Sood, A., Hayes, D.K., Sanchez, R.G., 2015. Neutron noise measurements on HEU foils moderated by lucite. In: 2015 American Nuclear Society Annual Meeting, San Antonio TX.

Hutchinson, J., et al., 2015. Estimation of uncertainties for subcritical benchmark measurements. In: International Conference on Nuclear Criticality.

Hutchinson, J. et al., 2016. Subcritical multiplication experiments & simulations: Overview and recent advances, Advances in Nuclear Nonproliferation Technology and Policy Conference.

Hutchinson, J., Bahran, R., Cutler, T., et al., 2017. Subcritical copper-reflected α-phase plutonium (scrαp) measurements and simulations. In: International Conference on Mathematics and Computational Methods Applied to Nuclear Science and Engineering, LA-UR-17-20621.

Iyer, R.H., Naik, H., Pandey, A.K., Kalsi, P.C., Singh, R.J., Ramaswami, A., Nair, A.G.C., 2000. Measurement of absolute fission yields in the fast neutron-induced fission of actinides: ^{238}U, ^{237}Np, ^{238}Pu, ^{240}Pu, ^{243}Am, and ^{244}Cm by track-etch-cum-gamma spectrometry. Nucl. Sci. Eng. 135, 227–245.

Knoll, G.F., 2010. Radiation Detection and Measurement. Wiley.

Lestone, J., 2005. Energy and isotope dependence of neutron multiplicity distributions. Nucl. Sci. Eng.

Madland, D.G., Nix, J.R., 1982. New calculation of prompt fission neutron spectra and average prompt neutron multiplicities. Nucl. Sci. Eng. 81, 213–271.

Mattingly, J., 2009. Polyethylene-reflected plutonium metal sphere: Subcritical neutron and gamma measurements, Sandia National Laboratory Report SAND2009-5804.

MCNP6™ User's Manual, Version 1.0, May 2013.

Miller, E.C., 2012. Characterization of Fissionable Material using a Time-correlated Pulse-height Technique for Liquid Scintillators. University of Michigan (PhD Thesis).

Miller, E.C., Mattingly, J.K., Dennis, B.D., Clarke, S.D., Pozzi, S.A., 2010. Simulations of neutron multiplicity measurements with MCNP-PoliMi, Technical Report SAND2010-6830, Sandia National Laboratory, 2010.

Moss, C., Sorenson, E., Nelson, M., 2016. Multiplicity Counter-15 (MC-15) User Manual, Los Alamos National Laboratory, LA-UR-16-27099.

Naika, H., Mulikb, V., Prajapatic, P., Shivasankard, B., Suryanarayanae, S., Jagadeesanf, K., Thakaref, S., Sharmae, S., Goswamia, A., 2013. Mass distribution in the quasi-mono-energetic neutron-induced fission of ^{238}U. Nucl. Phys. A 913, 185–205.

NRDC-Network, 2017. CSISRS/EXFOR library of experimental cross sections,www.nndc.bnl.gov/exfor.

Padovani, E., Pozzi, S.A., Clarke, S.D., Miller, E.C., 2012. MCNPX-PoliMi User's Manual, C00791 MNYCP, Radiation Safety Information Computational Center. Oak Ridge National Laboratory.
Pozzi, S. et al., 2012. MCNPX-PoliMi for nuclear nonproliferation applications. Nucl. Instrum. Methods Phys. Res., Sect. A 694, 119–125.
Pozzi, S.A., Padovani, E., Marseguerra, M., 2003. MCNP-PoliMi: a Monte Carlo code for correlation measurements. Nucl. Instrum. Methods Phys. Res. A 513, 550–558.
Richard, B., Hutchinson, J., 2016. Tungsten-reflected plutonium-metal-sphere subcritical measurements. In: International Handbook of Evaluated Criticality Safety Benchmark Experiments, NEA/NSC/DOC/(95)03/I, FUND-NCERC-PU-HE3-MULT-002.
Richard, B., et al., 2016. Nickel-reflected plutonium-metal-sphere subcritical measurements. In: International Handbook of Evaluated Criticality Safety Benchmark Experiments, NEA/NSC/DOC/(95)03/I, FUND-NCERC-PU-HE3-MULT-001.
Rising, M., et al., 2014. Correlated neutron and gamma-ray emissions in MCNP6, 2014 ANS Winter Meeting and Nuclear Technology Expo.
Rising, M., 2013. Evaluation and uncertainty quantification of prompt fission neutron spectra of uranium and plutonium isotopes. Nucl. Sci. Eng. 175 (1), 81–93.
Santamarina, A., Bernard, D., Blaise, P., et al., 2009. The JEFF-3.1.1 nuclear data library, JEFF Report 22.
Santi, P., Miller, M., 2008. Reevaluation of prompt neutron emission multiplicity distributions for spontaneous fission. Nucl. Sci. Eng. 160, 190–199.
Shibata, K., Iwamoto, O., Nakagawa, T., Iwamoto, N., Ichihara, A., Kunieda, S., Chiba, S., Furutaka, K., Otuka, N., Ohsawa, T., Murata, T., Matsunobu, H., Zukeran, A., Kamada, S., Katakura, J., 2011. JENDL-4.0: A new library for nuclear science and engineering. J. Nucl. Sci. Technol. 48 (1), 1–30.
Smith-Nelson, M., 2015. Momentum: version 0.36.3, LANL Software.
Sood, A., Solomon, C.J., Hutchinson, J.D., Bahran, R., 2014. A review of recent R&D efforts in sub-critical multiplication measurements and simulations. In: Transactions of the American Nuclear Society Annual Meeting, 2014.
Talou, P. et al., 2013. Prompt fission neutrons and gamma rays in a Monte Carlo Hauser-Feshbach formalism. Phys. Procedia 47, 39–46.
Terrell, J., 1957. Distributions of fission neutron numbers. Phys. Rev. 108, 783–789.
Trahan, A., 2016. Utilization of the Differential Die-away Self-interrogation Technique for Characterization of Spent Nuclear Fuel. University of Michigan (Ph.D. thesis).
Verbeke, J., Randrup, J., Vogt, R., 2015. Fission reaction event yield algorithm, FREYA – for event-by-event simulation of fission. Comput. Phys. Commun. 191, 178–202.
Verbeke, J.M., Randrup, J., Vogt, R., 2016. Fission reaction yield algorithm FREYA user manual 2.0, Lawrence Livermore National Laboratory report LLNL-SM-705798.
Wagemans, C., 1991. The Nuclear Fission Process. CRC Press, Boca Raton.